ABSTRACT

Title of Document: INTEGRATION OF A THERMOELECTRIC SUBCOOLER INTO A CARBON DIOXIDE TRANSCRITICAL VAPOR COMPRESSION CYCLE REFRIGERATION SYSTEM

Jonathan Michael Schoenfeld, Master of Science, 2008

Directed By: Professor and Director of the Center for Environmental Energy Engineering, Dr. Reinhard Radermacher, Mechanical Engineering

A thermoelectric (TE) subcooler was designed and fabricated to subcool CO_2 exiting a gas cooler of a transcritical vapor compression cycle test system. The thermoelectric modules operated at efficiencies greater than the baseline system, increasing capacity and the overall coefficient of performance (COP) of the entire system. Subcooling of the CO_2 before the expansion device led to a reduced optimum high side pressure, resulting in greater COP improvement that cannot be achieved in conventional refrigerant vapor compression systems utilizing a TE Subcooler. Improvements in COP of 10% were demonstrated with a corresponding capacity increase of 13%. A capacity increase of 24% was demonstrated at a comparable COP as the baseline system. Theoretical analysis of a combined Expander-TE Subcooler system, in which the electric power required by the TE Subcooler is provided by an expander-generator, was shown to provide a 30% increase in COP with a corresponding 24% increase in capacity.

INTEGRATION OF A THERMOELECTRIC SUBCOOLER INTO A CARBON DIOXIDE TRANSCRITICAL VAPOR COMPRESSION CYCLE REFRIGERATION SYSTEM

By

Jonathan Michael Schoenfeld

Thesis submitted to the Faculty of the Graduate School of the
University of Maryland, College Park, in partial fulfillment
of the requirements for the degree of
Master of Science
2008

Advisory Committee:
Professor Reinhard Radermacher, Chair
Professor Avram Bar-Cohen
Professor Bao Yang

© Copyright by
Jonathan Michael Schoenfeld
2008

Dedication

This work is dedicated to the memory of my grandfather, Dr. Robert Schoenfeld, and his legacy of intellectual honesty, trust in human reason, and belief that a better world is possible if we are willing to struggle for it.

Acknowledgements

This work was made possible by the Center for Environmental Energy Engineering at the University of Maryland and the Alternative Cooling Technologies & Applications Consortium. Special thanks to Dr. Reinhard Radermacher and Dr. Yunho Hwang for their continued guidance throughout the project as well as Jan Muehlbauer and Dr. Serguei Dessiatoun whose assistance was indispensable.

Table of Contents

Dedication ii
Acknowledgements iii
Table of Contents iv
List of Tables vi
List of Figures vii
List of Abbreviations and Nomenclature ix
Chapter 1: Introduction 1
  1.1: Thermoelectric Cooling 1
  1.2: Literature Review 3
    1.2.1: Thermoelectrics 3
    1.2.2: Carbon Dioxide Transcritical Refrigeration Systems 7
    1.2.3: Thermoelectric Subcooler 8
  1.3: Objective 10
Chapter 2: Approach 11
  2.1: TE Subcooler Design 11
    2.1.1: TE Subcooler Basics 11
    2.1.2: TE Subcooler Modeling 15
    2.1.3: CO_2 Microchannel 19
    2.1.4: Thermosyphon Evaporator 24
    2.1.5: Thermal Interface Material 27
    2.1.6: TE Subcooler Assembly 28
  2.2: Experimental Setup 30
    2.2.1: CO_2 System 30
    2.2.2: Measurement and DAQ System 34
    2.2.3: Energy Balance 37
    2.2.4: Test Matrix 38
Chapter 3: Results and Discussion 40
  3.1: Experimental Results 40
    3.1.1: Preliminary Testing 40
    3.1.2: First Generation Subcooler (Round 1) 42
      3.1.2.1: System performance 42
      3.1.2.2: TE Subcooler Performance 45
    3.1.3: First and Second Generation Subcooler (Round 2) 49
      3.1.3.1: System Performance 50
      3.1.3.2: TE Subcooler Performance 52
    3.1.3: First and Third Generation Subcooler (Round 3) 59
      3.1.3.1: System Performance 59
      3.1.3.2: TE Subcooler Performance 61
  3.2: Modeling Results 71
    3.2.1: TE Subcooler Performance Enhancement 71
    3.2.2: Expander-TE Subcooler System 75
Chapter 4: Conclusions and Future Work 79

4.1: Conclusions 79
4.2: Recommendations for Future Work 85
4.3: Summary of Completed Tasks and Key Findings 86
Bibliography 88

List of Tables

Table 1: Measurement device uncertainties. 37
Table 2: Test Matrix 39
Table 3: Baseline and TE Subcooler system performance at a suction pressure of 4,198 kPa. 43
Table 4: System performance at a suction pressure of 2,906 kPa. 50
Table 5: Parameter assumptions for ΔT calculation. 58
Table 6: System performance during third round of testing. 60
Table 7: Parameter assumptions for ΔT calculation. 70
Table 8: Theoretical system performance with improved TE Subcooler design. 75
Table 9: System assumptions 76
Table 10: COP and capacity of four different systems 77

List of Figures

Figure 1: Schematic of a thermoelectric couple. 2
Figure 2: Pressure-enthalpy diagram for a CO_2 transcritical cycle with and without a TE Subcooler. 9
Figure 3: Contributing factors to the temperature difference across the TE module.. 12
Figure 4: Marlow Industries, HWD0500-4040, thermoelectric modules and performance curves. 13
Figure 5: Effect of port diameter on temperature difference between microchannel walls and CO_2. 20
Figure 6: Further reduction in convective temperature difference due to a reduced microchannel width. 21
Figure 7: Estimated system performance improvement with different module designs. 22
Figure 8: Copper microchannel heat exchanger. 23
Figure 9: Thermosyphon evaporator enhanced boiling surface for the second generation subcooler. 25
Figure 10: Micro Deformation Technology enhanced boiling surface from Wolverine Tube, Inc. 26
Figure 11: Third generation subcooler. 29
Figure 12: Diagram of the second generation subcooler with thermocouples............ 30
Figure 13: Schematic of the experimental setup 31
Figure 14: Round 1 TE Subcooler setup. 33
Figure 15: Testing rounds 2 and 3 TE Subcooler setup. 34
Figure 16: System COP for baseline system and with TE Subcooler at different supply current over a range of discharge pressures. 40
Figure 17: TE Subcooler COP at different supply current over a range of discharge pressures. 41
Figure 18: Gas Cooler (GC) outlet temperature for baseline and TE Subcooler system testing at different supply currents over a range of pressures. 42
Figure 19: System performance response to discharge pressure. 44
Figure 20: Pressure - enthalpy plot for the baseline system, TE System with maximum COP, and TE System with maximum capacity 45
Figure 21: First Generation TE Subcooler performance at a compressor discharge pressure of ~9,040 kPa. 46
Figure 22: First Generation TE Subcooler fluid temperatures.. 47
Figure 23: Specific heat of supercritical CO_2 versus temperature at various gas cooler pressures. 48
Figure 24: TE Subcooler performance dependence on discharge pressure. 49
Figure 25: System COP for the baseline and TE Subcooler cases over a range of pressures. 51
Figure 26: System capacity for the baseline and TE Subcooler systems.................... 51
Figure 27: TE COP and Capacity for the first and second generation subcoolers for the low temperature cooling application at the low discharge pressure. 52
Figure 28: Module and heatexchanger surfaces after dissassembly of the Second Generation Subcooler. 53

Figure 29: Voltage drop for each module along both the first and second generation subcoolers connected in parallel with a supply current of 4 amperes........................ 54
Figure 30: Temperature profile across second generation subcooler at 6 A and ~7900 kPa discharge pressure.. 55
Figure 31: Estimated module performance over the TE subcooler. 56
Figure 32: Calculated Reynolds and Prandtl numbers at each module of the TE Subcooler. 57
Figure 33: Contributing temperature differences across the TE Subcooler............... 59
Figure 34: System COP for the third round of testing... 60
Figure 35: System capacity for the third round of testing. 61
Figure 36: Pressure - enthalpy plot for the baseline system and combined 1st and 3rd generation TE Subcoolers at supply currents of 3A and 7.5A................................... 61
Figure 37: Performance of the first and third generation subcooler at a discharge pressure of 9200 kPa and a supply current of 4 Amps. 62
Figure 38: Third generation and first and third generation TE Subcooler performance versus supply current. 63
Figure 39: Thermosyphon thermal resistance versus heat rejection rate................... 65
Figure 40: Module voltage drop and CO_2 temperature... 66
Figure 41: Temperature profile along the third generation subcooler....................... 67
Figure 42: Module TE COP and Capacity for the third generation subcooler. 68
Figure 43: Temperature difference contributions for the third generation subcooler. 70
Figure 44: Calculated versus measured TE capacity and TE COP for the third generation subcooler. 72
Figure 45: Schematic diagram of a refrigeration system with an Expander-TE Subcooler. 76
Figure 46: Pressure-enthalpy chart for four different systems with and without a TE Subcooler and an expander. 78
Figure 47: Contributions to the total system COP from the baseline and TE Subcooler. 81

List of Abbreviations and Nomenclature

$\overline{C_p}$	Mean specific heat (J/kgK)
C_p	Specific heat (J/kgK)
CEEE	Center for Environmental Energy Engineering
COP	Coefficient of performance
ECU	Expander compressor unit
EDM	Electrical discharge machining
EES	Engineering Equation Solver
Gr	Grashof Number
GWD	Global warming potential
h	Specific enthalpy (J/kg)
HTC	Heat transfer coefficient (W/m^2K)
HFC	Hydroflourocarbon
I	Supply current (A)
k	Thermal conductivity (W/mK)
$\dot{m}$	Mass flow rate (kg/s)
MAM	Micro-alloyed-material
MFR	Mass flow rate
MLQW	Multi-layer quantum well
MTD	Maximum temperature difference
N	Number of couples
Nu	Nusselt Number
OCR	Oil circulation rate
P	Power (W)
Q_C	Module cooling capacity (W)
Q_H	Module heat rejection rate (W)
R	Thermal resistance (K/W)
Re	Reynolds Number
SLHX	Suction line heat exchanger
t	Thickness (m)
ΔT	Temperature difference (K)
T	Temperature (°C)
TCT	Two-phase closed type (thermosyphon)
TEC	Thermoelectric cooler
TLT	Two-phase loop type (thermosyphon)
V	Voltage drop (V)
Z	Figure of merit (1/K)
ZT	Non-dimensional figure of merit

Greek Symbols

α	Seebeck coefficient (V/K)
λ	Ratio of element height to cross-sectional area (1/m)
ρ	Fluid density (kg/m^3)

ρ_e	Electric resistivity (Ωm)
η	Efficiency

Subscripts

amb	Ambient
b	Bulk mean temperature
C	Cold side of TE module
cmp	Compressor
cond	Condenser
CO_2	Carbondioxide
conv	Convection
EB	Enhanced boiling surface
evap	Evaporator
Exp	Expander
gen	Generator
H	Hot side of TE module
hf	Heat rejection fluid
i	Module number
in	Inlet
ind	Indicated
m	TE Module
mat	Material
mc	Microchannel
mech	Mechanical
PB	Pool boiling
s	Isentropic
suct	Suction
sys	System
TE	Thermoelectric
TIM	Thermal interface material
vol	Volumetric
w	Microchannel wall

Chapter 1: Introduction

1.1: Thermoelectric Cooling

Thermoelectric coolers (TECs) are an attractive option for many cooling applications. TECs have no moving parts, making them reliable and silent in operation. They can provide localized cooling where it is needed most and are especially useful where there are size and weight constraints, such as electronics cooling. Vapor compression cycle cooling systems cannot operate easily in micro-gravitational environments or at extremely low temperatures, which makes TECs a viable option for space and cryogenic applications. Finally, as the international community continues to move towards alternatives to hydroflourocarbon (HFC) refrigerants used in vapor compression cycle cooling due to their global warming effects, TECs have the potential to fill that role as well.

Thermoelectric cooling is a result of the Peltier effect, in which heat absorbed or emitted from the junction of two semiconductors depending on the direction of an applied electric current. A thermoelectric couple consists of an electrical junction between two semiconductors with opposite Seebeck coefficients in which a DC current is applied. Figure 1 shows a schematic of a single thermoelectric couple. The semiconductors or thermoelectric material is of either n-type or p-type. In an n-type semiconductor a thermal drift flux (Gurevich and Logvinov, 2005) [1] proportional and opposite in direction to the applied current will develop while in a p-type semiconductor the thermal drift flux develops in the same direction. Because of this the junction of the two semiconductors is heats up or cools depending on the direction of the current.

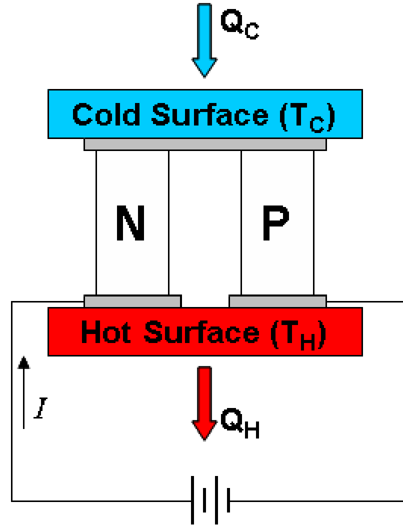

Figure 1: Schematic of a thermoelectric couple.

A thermoelectric module consists of several thermoelectric couples connected electrically in series and thermally in parallel. A thin ceramic plate, which is electrically insulating and thermally conductive, is placed on both the cold and hot side electric junctions. Through the Peltier effect a thermoelectric module is able to pump heat from the cold surface to the hot surface. Lessening the Peltier effect is the heat generated from joule heating within the semiconductors and thermal conduction from the hot side of the module. The total cooling capacity of the cold side and the heat rejection of the hot side of a thermoelectric module can be estimated from Equation 1 and 2, respectively. The electric power supplied to a thermoelectric module is given by Equation 3, which is equal to $Q_H - Q_C$.

$$Q_C = 2N\alpha I T_C - \frac{1}{2} I^2 2N\lambda\rho_e - \left(\frac{2N}{\lambda}\right) k(T_H - T_C) \quad \textbf{(1)}$$

$$Q_H = 2N\alpha I T_H + \frac{1}{2} I^2 2N\lambda\rho_e - \left(\frac{2N}{\lambda}\right) k(T_H - T_C) \quad \textbf{(2)}$$

$$P_{TE} = 2N\left(\alpha(T_H - T_C) + I\lambda\rho_e\right)I \quad \textbf{(3)}$$

In Equations 1 – 3 I is the supply current, α is the Seebeck coefficient, ρ_e is the electrical resistivity, and k is the thermal conductivity of the semiconductor. The parameters N and λ are the number of thermoelectric couples within the module and the ratio of the thermoelectric element length to cross-sectional area, respectively. The temperatures are denoted by T_C and T_H for the cold and hot surface, respectively. Equation 1 and 2 are idealizations as the radiation and convection within the pockets between the semiconductors is neglected (Nabi and Asias, 2005, [2]). As the temperature difference across the module ($\Delta T_m = T_H - T_C$) increases so does the heat transfer from the hot side of the module, thus reducing the cooling capacity of the module. It is assumed that half the heat produced by the joule heating effect contributes to the heating of each side of the TE module. As the current increases the joule heating effect decreases the cooling capacity of the cold side and increases the heat rejection of the hot side of the module. The value of λ is generally optimized for a particular application in order to minimize the negative effects of conduction and joule heating.

1.2: Literature Review

1.2.1: Thermoelectrics

There are two general research areas focused on increasing TEC performance; materials research on thermoelectric semiconductors and system level assembly and heat dissipation techniques. The former is focused on developing advanced thermoelectric materials with superior thermoelectric properties. The most important parameter of a thermoelectric semiconductor is the figure of merit, Z, which is given by $\alpha^2/(k\rho_e)$. Each of these properties is temperature dependent so often the figure of merit will be given at a

particular temperature in the dimensionless form, ZT. Increasing the figure of merit directly results in an increase in the optimum COP of a TEC. The most common thermoelectric semiconductor in today's TECs is Bismuth Telluride (Bi_2Te_3), which has a ZT of ~0.9 at 300 K. Bass et al. (2004) [3] investigated the use of multi-layer quantum well (MLQW) thermoelectrics in a cooling application. MLQW thermoelectric material is a composite of thin layers of alternating semiconductor material with differing electronic band gaps deposited on a substrate. In this way, the thermal and electrical conductivity of the material can be decoupled. The non-dimensional figure of merit of such composite materials has been determined experimentally to be as high as 3 or 4. Theoretical analysis predicted COPs as high as 5 at a ΔT_m of 20 K. A TEC utilizing MLQW thermoelectric material is still under development. It can be expected that the additional manufacturing costs of such a module would be substantial.

Other efforts to improve the figure of merit of thermoelectric materials have been focused on nanotechnology (Goldsmid, 2006) [4]. By reducing the dimensions to a certain degree it is possible to change the electronic band structure of a material, which leads to a change in the thermoelectric properties. Bismuth, which was the first material to display thermoelectric properties, may be able to reach a ZT of 4 when in the form of a nanowire. Besides the obvious increase in optimum COP provided by such an improvement in thermoelectric properties, it has also been recognized that Tellurium, a main component in Bismuth Telluride, is becoming increasingly rare and expensive, which will eventually lead to a necessary replacement for thermoelectric materials. Further research is still

required to develop nanotechnology thermoelectrics, with the ultimate hurdle being the fabrication of a scaled up module with an applicable cooling capacity.

On the system level side, the layering of thermoelectric modules offers performance improvements under certain conditions. Two-stage thermoelectric coolers, which utilize a second layer of thermoelectric elements, can increase the maximum temperature difference (MTD) between the sides of a TE module in which cooling still takes place. Xuan et al. (2002) [5] investigated different electrical configurations and the ratio of TE couples between the two stages. When each stage is powered independently a two stage TE cooler with an MTD greater than 100 K is achievable. The COP at these extremely large ΔTs is very low, but for cryogenic applications, this is not the chief concern.

The efficient use of TECs requires an effective heat sink for the hot surface and heat source for the cold surface in order to minimize the ΔT_m. Chein and Chen (2005) [6] investigated the use of a microchannel heat sink on a TE module used to cool a water tank. The microchannels were etched into a silicon wafer with a glass cover plate. Four microchannel heat exchangers were fabricated with a differing number of ports and hydraulic diameters (D_h), from 89 ports at a D_h of 65 μm to 44 ports at a D_h of 150 μm. Water was pumped at flow rates ranging from 289 – 10,702 ml/h to remove the heat from the hot side of the module. The microchannel was placed on top of a 4 cm x 4 cm TE module. The lowest measured thermal resistance for the heat sink was 1.68 K/W. The authors suggested that the thermal resistance could be reduced to 0.5 K/W by increasing

the aspect ratio of the microchannel ports and by using a more conductive material like copper.

Webb et al. (1998) [7] investigated the use of a thermosyphon as the heat sink of a TE module used for electronics cooling. A porous aluminum surface was employed to enhance the boiling heat transfer in the evaporator. The condenser was constructed with internal microfins to enhance condensation. An experimental study was conducted with simulated heat loads typical of a thermoelectric module heat rejection. At 75 W a thermal resistance of 0.0505 K/W was calculated for a 45 mm square enhanced boiling surface. The authors also recognized that the thermal resistance decreased slightly with increasing heat flux.

As the figure of merit continues to increase through a continued research effort, the use of thermoelectrics for air cooling has become more feasible. Riffat and Qiu (2005) [8] investigated TE air conditioning systems with an air and water cooled heat sink. A cylindrical heat sink was designed through the optimization of the interior fin length and pitch as well as fluid velocity. The cylindrical design was capable of reducing heat exchanger volume and thermal resistance. An evaporative water “condenser” was suggested as the outdoor unit, which would cool the circulated water down close to the wet bulb temperature through convective and evaporative cooling. It was shown that the thermal resistance of a water cooled heat sink was significantly lower than an air cooled heat sink, with values reported as low as 4.75×10^{-4} K/W for a cylinder with an outer surface area of 0.23 m^2. An ideal COP of 1.8 was reported at a ΔT_m of 20 K assuming a

figure of merit of $Z = 3.0 \times 10^{-3}\ K^{-1}$. Although possible, it would be difficult to fabricate a TE module on a curved surface as suggested.

1.2.2: Carbon Dioxide Transcritical Refrigeration Systems

An international research focus on vapor compression cycles using natural refrigerants has emerged due to the global warming potential (GWP) of HFCs. Carbon dioxide (CO_2) is a particularly attractive alternative to conventional refrigerants because it has a relatively low GWP; is nontoxic and non-flammable; and has a high volumetric capacity. Unfortunately, the CO_2 transcritical cycle is inherently less efficient than an HFC subcritical cycle due in part to the large pressure difference between the high and low side pressures at high ambient temperatures.

One method to increase the efficiency of a CO_2 system is to use an expander as an expansion device instead of an orifice tube or thermostatic expansion valve. An Expander Compressor Unit (ECU) recovers a portion of the throttling losses during the expansion process to drive part of the compression process. Additionally, the enthalpy of the refrigerant at the expander outlet is less than it would be if an isenthalpic expansion device were employed. The decreased enthalpy entering the evaporator increases the capacity of the system. An improvement in COP of about 30% has been demonstrated experimentally by Kohsokabe et al. (2006) [9].

Another method employed to increase the efficiency of CO_2 systems is a suction line heat exchanger (SLHX). A SLHX exchanges heat between the exit of the gas cooler and the

suction line of the compressor. Boewe et al. (1999) [10] demonstrated COP and capacity improvements of 26% and 10%, respectively under idling conditions in an automotive application. The disadvantages to SLHXs are that increased superheat at the compressor suction increases the compressor power and discharge temperature. Under driving conditions, discharge temperatures exceeded 140ºC, which was determined to be the upper limit due to material constraints.

<u>1.2.3: Thermoelectric Subcooler</u>

Typically, conventional vapor compression air conditioning systems operate at a higher COP over a larger temperature difference than TECs can currently operate. Winkler et al. (2006) [11] [34] recognized that thermoelectric modules could be employed at the outlet of a condenser to reduce the refrigerant temperature to below the ambient temperature. In this way the thermoelectric modules would operate with a smaller ΔT_m and at higher efficiency. The heat removed from the refrigerant results in a direct increase in the capacity of the vapor compression system by reducing the enthalpy entering the evaporator. In a transcritical cycle the high side pressure is optimized for a particular working fluid temperature entering the expansion device. By subcooling the working fluid the high side pressure can be reduced, increasing compressor efficiency and decreasing compressor power. The thermoelectric (TE) Subcooler is well suited to increase both the COP and capacity of CO_2 transcritical cycle for that reason. Figure 2 illustrates this advantage on a pressure-enthalpy diagram. Through theoretical means, Winkler et al. (2006) [11], suggested that a 16% COP improvement with a greater than 20% improvement in capacity was possible in a CO_2 system.

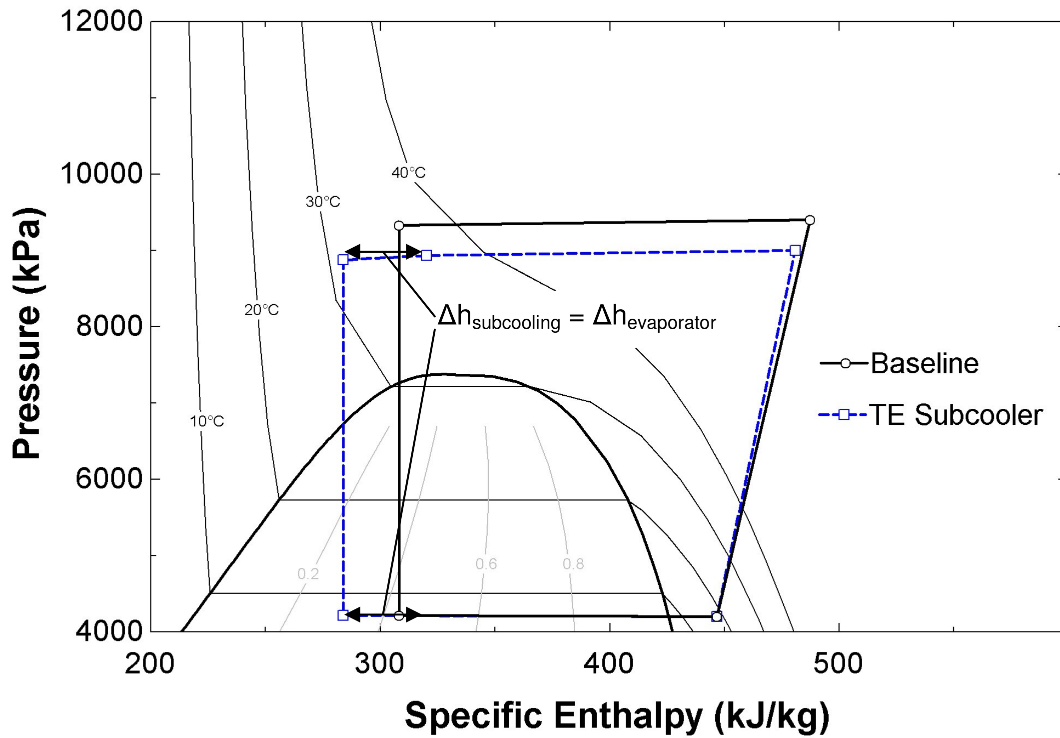

Figure 2: Pressure-enthalpy diagram for a CO_2 transcritical cycle with and without a TE Subcooler.

Muehlbauer (2006) [12] investigated the effects of a TE Subcooler on a R410A air conditioning system with a cooling capacity of about 10 kW. The TE Subcooler was assembled from aluminum microchannel heat exchangers with the TE modules sandwiched in between. Two heat rejection mediums were investigated. Water was utilized in a closed loop employing a circulation pump to drive the water from the TE Subcooler to a microchannel heat exchanger, utilizing a separate set of fans. The second and more successful strategy used a thermosyphon loop with R22 as the working fluid. A large automotive condenser was utilized with a separate pair of fans to reject the heat to the ambient. Capacity increases were demonstrated at about 5%, but no significant increases in system COP were realized. Through a theoretical analysis it was established that along with the supply current, the number of modules, or total capacity, must also be

optimized to achieve the full potential of the TE Subcooler. In order to demonstrate COP improvements the capacity of the TE Subcooler would need to be significantly greater.

1.3: Objective

There are three objectives to this project. The first is to design and fabricate a TE Subcooler. The second is to experimentally test and verify the performance improvement potential of the TE Subcooler in a small transcritical CO_2 refrigeration system. The third and final objective is to assess the theoretical potential of a TE Subcooler powered by an expander.

Two TE Subcoolers were designed and fabricated for testing within a small CO_2 system. One preexisting design was also tested. The capacity and COP of the CO_2 system and TE Subcoolers were compared. The TE Subcooler performance was analyzed in order to determine the significance of the contributing thermal barriers and develop possible design improvements. The theoretical potential performance of the TE Subcooler was then assessed. Additionally, the use of an expander to power the TE Subcooler was investigated through theoretical means.

Chapter 2: Approach

2.1: TE Subcooler Design

2.1.1: TE Subcooler Basics

A TE Subcooler consists of three main components, the TE modules, a cold side heat exchanger, and a hot side heat sink. The cold side heat exchanger transfers heat from the working fluid, in this case CO_2, to the cold side of the TE module. The lower the thermal resistance of this heat exchanger, the higher the temperature of the cold surface can be while still providing cooling to the CO_2. The hot side heat sink rejects the heat from the TE modules to the ambient. The lower the thermal resistance of this heat exchanger, the lower the temperature of the hot side surface. Between each heat exchanger and the TE modules is an interface which also has an associated thermal resistance.

The goal of the TE Subcooler design is to minimize the temperature difference across the thermoelectric modules by minimizing all thermal resistances. There are five contributing thermal barriers: convection to the CO_2 from the wall of the CO_2 heat exchanger, conduction through the heat exchanger materials, conduction through the thermal interface material, convection to the heat rejection fluid, and the temperature difference between the two fluids. Figure 3 illustrates five contributing factors to the temperature difference across the thermoelectric module.

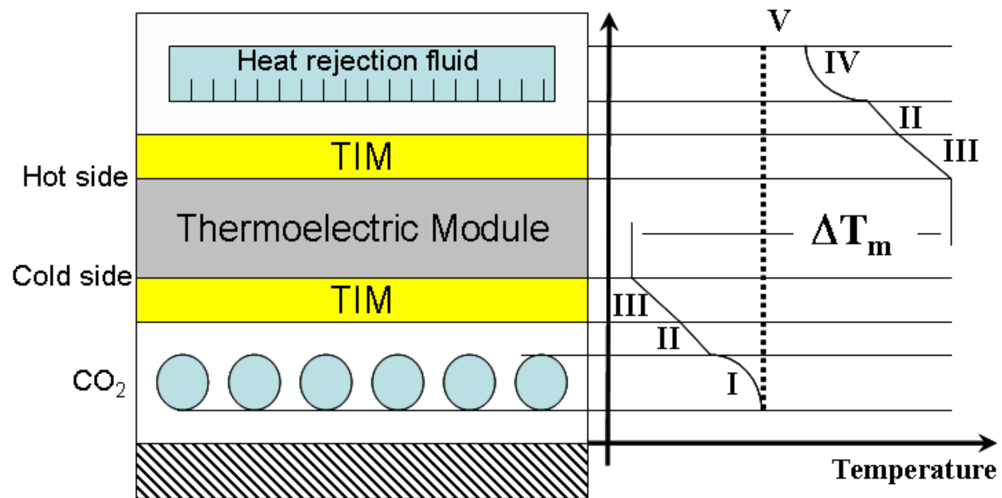

Figure 3: Contributing factors to the temperature difference across the TE module.

The TE modules (Figure 4a) utilized in each of the TE Subcoolers were donated by Marlow Industries. The thermoelectric semiconductor is a micro-alloyed-material (MAM) Bismuth Telluride with a ZT of approximately 0.9 at 300 K. By reducing the grain size of the material, Marlow was able to achieve the same thermoelectric properties of bulk Bismuth Telluride with improved strength and durability. The modules are approximately 4 cm by 4 cm and 1.2 mm thick, with 128 element pairs or couples. The ceramic plates are constructed out of Beryllium Oxide, with printed electrical junctions connecting the n and p-type elements. Power is supplied through electrical connections made with the copper electrical leads. The minimum recommended flatness of the heat exchanger mated with the Beryllium Oxide ceramic plates is 0.025 mm/mm. Figure 4b shows the typical performance of the modules at a hot surface temperature of 50°C.

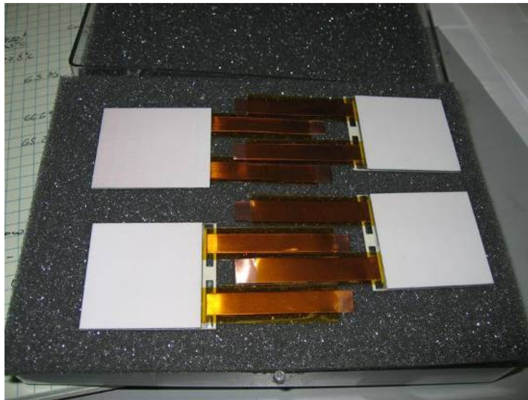

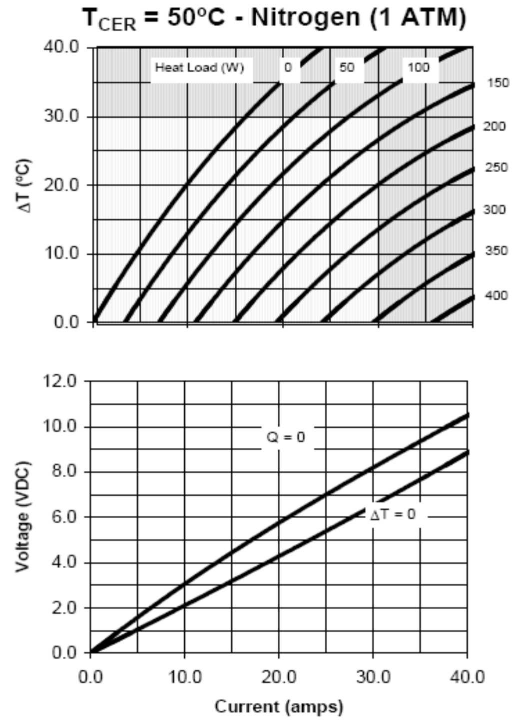

a) b)

Figure 4: a) Marlow Industries, HWD0500-4040, thermoelectric modules. b) Typical performance curves of HWD0500-4040 TE Modules.

Various options were explored for the cold side heat exchanger. A minimization of the thermal resistance of convection is equivalent to maximizing the product of the heat transfer coefficient (HTC) and the heat transfer surface area. Besides a minimization of thermal resistance, the CO_2 heat exchanger must be designed to withstand the high pressures used in a transcritical cycle. Additionally, oil circulation and pressure drop must also be considered. A direct contact heat exchanger offers the possibility of eliminating the thermal interface between the heat exchanger and the modules. Unfortunately, due to the high pressure of the CO_2, it would be extremely difficult to fabricate such a heat exchanger in a safe fashion. Additionally, the surface area of the CO_2 in contact with the TE module is less than that of a microchannel heat exchanger. Microchannel heat exchangers have a number of advantages over other designs including,

high heat transfer coefficients, safety at even extremely high pressures, and a large knowledge base. For these reasons it was decided to utilize a microchannel heat exchanger on the cold side.

Common methods to remove heat from the hot side of TE modules are air or water cooling, thermosyphons, and heat pipes. As described in Section 1.2.3 water cooled TE coolers have shown to be significantly more efficient than their air cooled counter parts. As discussed, in previous research conducted at the Center for Environmental Energy Engineering (CEEE), a thermosyphon was shown to outperform a water cooled system. Water cooled systems also require a water pump, which has additional power needs and adds heat to the water loop.

There are two main types of thermosyphons, two-phase closed type thermosyphons (TCT) and two-phase loop-type thermosyphons (TLT). In each case the flow is driven by gravity. As refrigerant boils in the evaporator the density decreases and the buoyant force causes it to rise to the condenser, at the same time condensed liquid in the condenser is driven by gravity back to the evaporator. In a TCT the vapor and condensate travel through the same piping in opposite directions. The counter-flow can reduce performance by increasing pressure drop. In TLT system vapor travels up through a vapor line to the condenser and drains back through a separate liquid line. In this way the refrigerant flows in a loop through the system. A TLT was selected for the heat rejection system because of its passive operation and low thermal resistance.

Initial testing was performed on the first generation TE Subcooler, which was designed in a previous study for use in a large conventional refrigerant air conditioning system. The subcooler consisted of a single aluminum microchannel CO_2 heat exchanger sandwiched in between two aluminum microchannel heat rejection heat exchangers. The TE modules were placed in between the CO_2 heat exchanger and the heat rejection heat exchangers, with five on each side for a total of ten modules. The port diameter and wall thickness of the microchannels was unknown during construction. From the thickness of the microchannel it was estimated that the port diameter was approximately 1.5 mm. A thermosyphon loop was employed to reject the heat from hot side of the modules.

<u>2.1.2: TE Subcooler Modeling</u>

The TE Subcooler was modeled in order to assess the performance improvements of different designs. Additionally, a simplified system model was developed to estimate the benefits of a TE Subcooler in a carbon dioxide transcritical system. Engineering Equation Solver (EES) was used to perform the thermodynamic calculations of the cooling systems in question.

The TE module product data sheet included performance curves as seen in Figure 4b at a hot surface temperature of 50°C and 85°C. The data for the heat pumping capacity was loaded into two lookup tables requiring any two of the three parameters, ΔT, supply current, and cooling capacity, in order to calculate the third. The performance of a singe module was estimated from a linear approximation from the two performance curves based on the TE hot side temperature.

For the voltage drop data, second degree polynomials were used to estimate the voltage as a function of supply current for the $\Delta T = 0$ and $Q = 0$ case as shown in Figure 4b. A linear approximation was then made between the two curves depending on the ratio of the ΔT and the maximum temperature difference (MTD) or $\Delta T_{Q=0}$. Finally, as in the cooling capacity curves a linear approximation estimates the voltage drop at the given TE hot side surface temperature. The power input is calculated as the supply current multiplied by the voltage drop.

This simplified approach was intended to give a first order approximation of the TE performance. Temperature dependence of the thermoelectric properties is not linear, but since the model was used to determine relative changes in performance this was an acceptable idealization. Additionally, the changes in hot side surface temperature were relatively small, <5 K, which reduces the error of a linear approximation.

The TE Subcooler was modeled as a series of TE modules with a working fluid heat exchanger attached to the cold side and a heat rejection fluid heat exchanger attached to the hot side of each element. At each module an energy balance was performed. It was assumed that there was a negligible amount of heat transfer in the axial direction tangent to the module surfaces. Equation 4 and 5 gives the relationship between the cooling capacity and temperature difference between the cold side surface temperature and the CO_2 temperature.

$$Q_{C,i} = \frac{1}{R_{C,i}}(T_{CO2,i} - T_{C,i}) \quad \textbf{(4)}$$

$$R_{C,i} = \frac{1}{HTC_{conv}A_{mc}} + \frac{t_{mat}}{k_{mat}A_{TE}} + \frac{t_{TIM}}{k_{TIM}A_{TE}} \quad \textbf{(5)}$$

Q_C is cooling capacity of the TE module, R_C is the total thermal resistance on the cold side of the module, T_{CO2} is temperature of the CO_2, and T_C is the temperature of the cold surface of the module. The subscript i refers to the module number. At the inlet of the subcooler i equals one and the temperature of the CO_2 is equal to that exiting the gas cooler. The total thermal resistance changes over the length of the subcooler solely due to the changing properties of the working fluid. This will be discussed in greater detail in Section 3.1.3.2. The enthalpy is calculated at the inlet of each module through Equation 6. The temperature is then determined from the enthalpy and pressure using the equation of state developed by Span and Wagner [29].

$$h_{CO2,i+1} = h_{CO2,i} - \frac{Q_{c,i}}{\dot{m}} \quad \textbf{(6)}$$

On the heat rejection side Equations 7 and 8 give the relationship between the heat rejection rate and temperature differences. The heat rejection rate, Q_H, is equal to the cooling capacity plus the electrical power input to the TE module given by the product of the supply current, I, and the sum of the TE module voltage drops, V. The temperature of the hot surface of the module is given by T_H. Since it is assumed that the heat is rejected to a refrigerant undergoing a phase change, the heat rejection fluid temperature, T_{hf}, remains constant for each module as the saturation temperature. The thermal resistance, R_H, changes only very slightly with the pool boiling heat transfer coefficient at a low heat flux.

$$Q_{H,i} = \frac{1}{R_{H,i}}(T_{H,i} - T_{hf})$$
$$Q_{H,i} = Q_{C,i} + I\sum V_i \quad \textbf{(7)}$$

$$R_H = \frac{1}{HTC_{PB}A_{EB}} + \frac{t_{mat}}{k_{mat}A_{TE}} + \frac{t_{TIM}}{k_{TIM}A_{TE}} \quad \textbf{(8)}$$

On both the cold and hot side of the module the thermal resistance is the sum of the thermal resistances of the convection to the associated fluid, the conduction through the heat exchanger material (subscript *mat*), and conduction through the thermal interface material (subscript *TIM*). The thicknesses and thermal conductivities are denoted by t and k, respectively. The heat transfer area of the microchannel, A_{MC}, is equal to the inner surface area of the microchannel. The heat transfer area of the enhanced boiling surface of the thermosyphon evaporator is denoted by A_{EB}, and is equal to the horizontal projection of the surface area. For all other cases the heat transfer area is assumed to be the area of the TE modules, A_{TE}. The heat transfer coefficient HTC_{conv} for the CO_2 within the microchannel was calculated using the Gnielinski [14] correlation with the Petukhov [15] correlation used to calculate the roughness factor. A correlation developed by Rohsenow (1952) [16] was used to give at least a rough estimate of the nucleate boiling heat transfer coefficient, HTC_{PB}.

Finally, the total ΔT_m across each TE module is calculated from Equation 9. When the working fluid inlet temperature, heat rejection fluid temperature, supply current, and all properties and dimensions are known the system of equations along with the performance curves described above can be solved to give the cooling capacity and COP of each TE module.

$$\Delta T_{m,i} = (T_{CO2,i} - T_{c,i}) + (T_{h,i} - T_{hf}) + (T_{hf} - T_{CO2,i}) \quad \textbf{(9)}$$

For the TE Subcooler design a simplified system model was developed. A constant flow rate of 10 g/s was assumed, with a constant compressor suction condition of 4,198 kPa and 11.1 K superheat. The gas cooler outlet was assumed to be constant as well at 40°C. The compressor power consumption was estimated to vary linearly with the discharge pressure based on previous data taken from the CO_2 compressor to be used in this study. The model was used only to assess the relative differences in COP and not to accurately predict system performance.

2.1.3: CO_2 Microchannel

The heat flux within the TE Subcooler microchannel can be an order of magnitude greater than the microchannels of a gas cooler or condenser. This results in a large temperature difference between the microchannel walls and the CO_2. The heat transfer coefficient and temperature difference was calculated for port diameters from 0.75 mm to 2 mm. The results can be seen in Figure 5 assuming a constant CO_2 temperature and pressure of 35°C and 10,000 kPa, respectively, and a heat transfer rate of 50 W per module. Since the CO_2 is a high density supercritical fluid within the TE Subcooler there is a minimal pressure drop penalty through the microchannel. By reducing the port diameter from 1.5 mm to 0.8 mm the temperature difference can be reduced by more than 2 K due to an increased heat transfer surface area to fluid volume ratio.

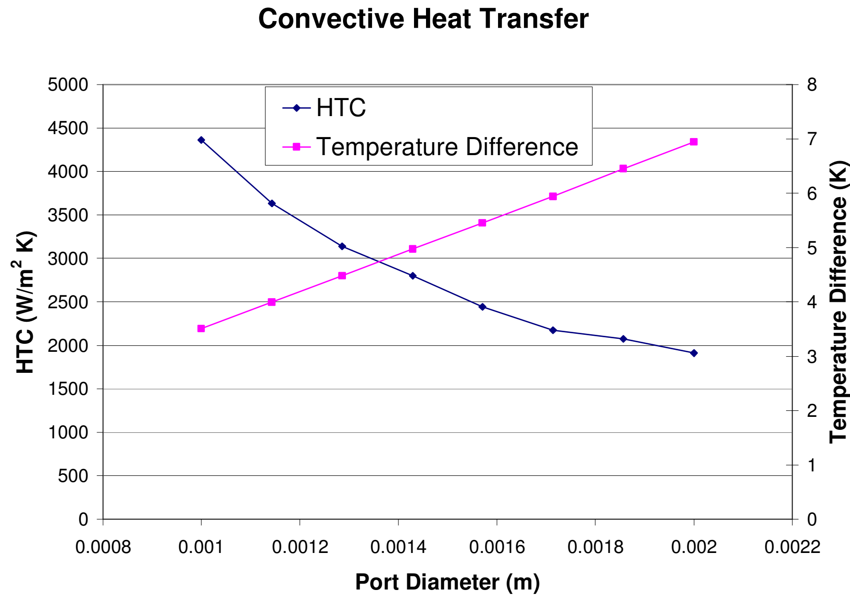

Figure 5: Effect of port diameter on temperature difference between microchannel walls and CO_2. *Heat transfer coefficient (HTC) calculated by the Gnielinski correlation.

Additional reduction in the temperature difference between the microchannel wall and the CO_2 can come from a decrease in heat flux. As described before the thermoelectric module is a collection of thermoelectric elements connected thermally in parallel. In order to reduce the heat flux the elements must be wider or spaced further apart which would increase the parasitic heat transfer decreasing module performance. A more detailed model of the TE modules is necessary to accurately assess the effects of a change in heat flux on the system.

The CO_2 microchannel should be approximately the same width as the TE modules. If the modules were constructed with a reduced width but the same area and cooling capacity, the number of ports within the microchannel would be reduced allowing for a greater mass flux and increased heat transfer coefficient. Figure 6 shows the further reduction in convective temperature difference achievable by a reduction in module width.

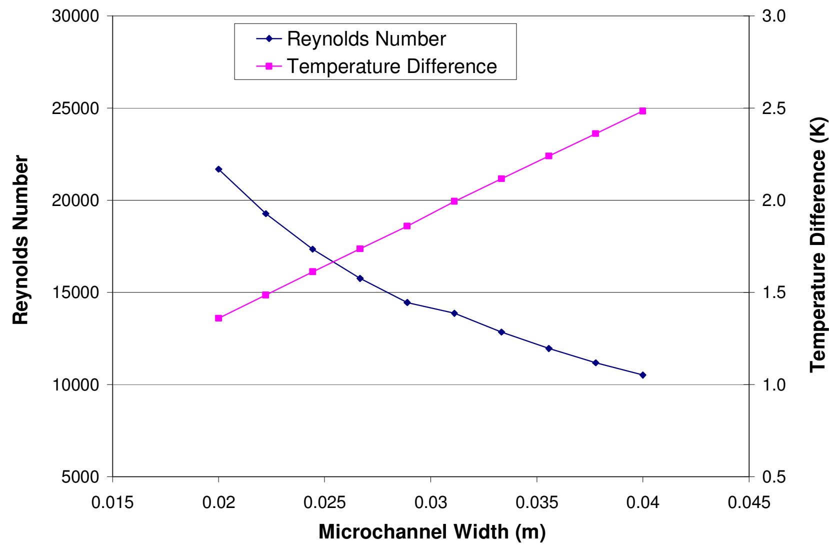

Figure 6: Further reduction in convective temperature difference due to a reduced microchannel width.

Using the model described above, four systems were compared with subcoolers consisting of 10 modules with different heat fluxes and widths. The module heat flux was either set to that of the standard modules described above or to a low heat flux, one half of the standard module by increasing the module area. It was assumed that the decreased heat flux did not negatively affect the performance of the modules. The width of the modules was set to the normal module width of 4 cm or a decreased width of 2 cm. The supply current and high side pressure were optimized in each case. Figure 7 shows the relative increase in system COP. Although, the low heat flux and module width case provides the greatest improvement, the COP increase from the standard modules is only about 6%. It is also important to recognize the modules would need to be 16 cm in length making the total TE Subcooler length approximately 1.6 m and requiring a heat rejection heat exchanger of the same size. It was decided that the difficulties in constructing heat

exchangers of the necessary size and in manufacturing custom modules were too great for the potential improvements in performance.

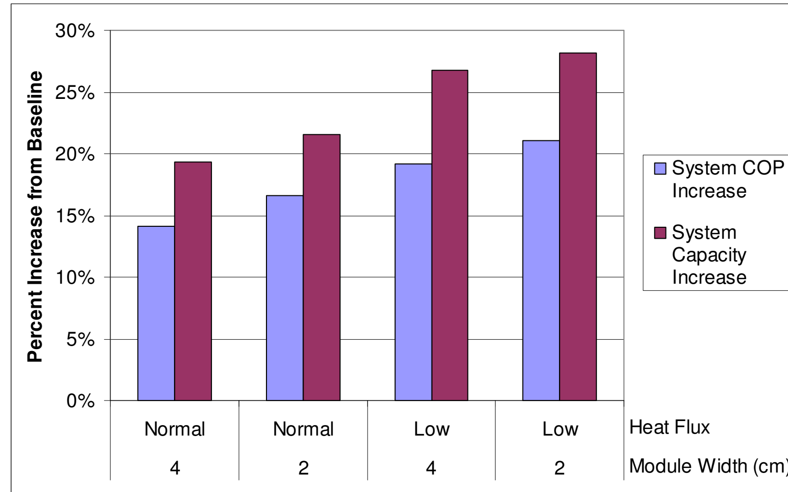

Figure 7: Estimated system performance improvement with different module designs.

Another fundamental difference between the microchannel heat exchanger required for a TE Subcooler and more traditional applications is the flatness and smoothness that is required. In order to limit the thermal contact resistance it is essential that the microchannel surface be as smooth and flat as possible to mate effectively with the flat TE modules. The first generation microchannels were constructed from Aluminum and although the surfaces were not perfectly flat, once a compressive force was applied the flexibility of the microchannel allowed for a sufficient mating surface. A new microchannel heat exchanger was fabricated at the University of Maryland for use in the second generation subcooler in an attempt to reduce the port diameter and improve upon the flatness from the previous TE Subcooler.

Several techniques to produce the microchannels with the required port diameter were investigated. Hole popping electrical discharge machining (EDM) has the ability to

produce holes of the necessary aspect ratio in a copper block, but was prohibitively expensive for the number of ports required in this study. Attempts at drilling 1.0 mm holes in a copper block were unsuccessful. Other options which included the use of a cover plate mated to a plate with shallow troughs were determined to be unsafe at the high pressures required by the system. Due to the inherent limitations of producing holes which were long enough and small enough an alternative method was utilized. Copper capillary tubing was purchased with an inner diameter of 0.8 mm. Fifteen tubes were brazed to copper headers and then brazed to a thin, flat copper plate which was to be mated with the TE modules. Figure 8 shows a picture of the completed copper microchannel heat exchanger.

Figure 8: Copper microchannel heat exchanger for second generation TE Subcooler.

The copper capillary tubing was brazed to the copper plate using a low temperature Silver-Copper alloy with Cadmium to reduce the likelihood of loosening the brazed connection to the headers. Pressure testing with a high pressure oil pump was performed to ensure safe operation at pressures up 15 MPa. During brazing to the copper capillary tubing the copper plate did undergo significant warpage. Unfortunately, there existed no reliable way to machine the copper plate flat without damaging the microchannels or the

brazed connections. The surface of the copper plate was sanded as flat as possible with a flat stone. Regardless, the surface could not be made as flat as originally intended.

Due to the inherent difficulties in fabricating microchannels and the results from the experiments which will be discussed in Section 3.1.3.2 the aluminum microchannel used to construct the first generation subcooler was utilized as the CO_2 heat exchanger for the third generation subcooler.

2.1.4: Thermosyphon Evaporator

The heat generated by the TE modules must be rejected to the ambient from the hot side of the TE Subcooler. To accomplish this efficiently a thermosyphon loop was employed. The thermosyphon evaporator boiling surface has a large impact on the temperature difference between the wall and the refrigerant. The pool boiling heat transfer coefficient of enhanced boiling surfaces is larger than plain surfaces due to the following [25][26][27]:

1. The bubble nucleation pores or cavities on enhanced surfaces are significantly larger than on plain surfaces, which cause a reduction in the required superheat.
2. Existence of thin film evaporation on enhanced surfaces is an extremely effective heat transfer mechanism.
3. There is convective heat transfer to liquid refrigerant pumped into the enhanced surface to take the place of departing vapor. This also preheats the refrigerant from the bulk refrigerant temperature.
4. The wetted surface of enhanced surfaces is significantly larger than plain surfaces.

Typical enhanced boiling surfaces range from abrasive treatments to reentrant cavities to lattice structures. One of the most simple yet still effective surfaces consists of open grooves. Bonilla et al. (1965) [25] showed an increase in the boiling coefficient by 100% over a polished surface.

For the second generation subcooler a 120 cm^2 enhanced boiling surface was machined on a copper plate. The surface consisted of 0.035 inch (0.889 mm) grooves cut to a depth of 0.10 inches (2.54 mm), spaced 0.04 inches (1.016 mm) apart. Figure 9 shows a picture of the enhanced boiling surface of the thermosyphon evaporator. The surface is similar to that of a low fin density with 13 fins per inch (fpi).

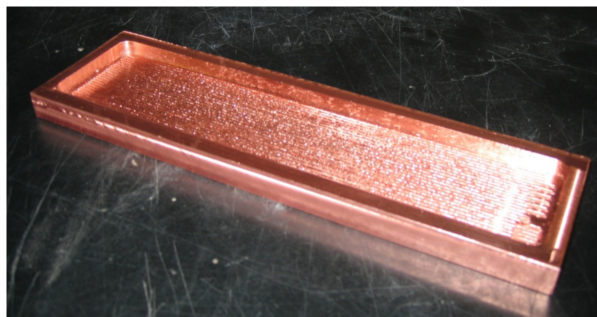

Figure 9: Thermosyphon evaporator enhanced boiling surface for the second generation subcooler.

For the third generation subcooler a microfinned enhanced boiling surface was prepared by Wolverine Tube, Inc. The Micro Deformation Technology was capable of producing 75 fins per inch on a 1/8th inch (3.175 mm) thick copper plate over a surface area of 105.8 cm^2. The successful fabrication of the boiling surface was the first time this technique had been performed on a plate with a thickness this large. Figure 10 shows a picture of the enhanced boiling surface. The surfaces of both subcoolers were purposefully designed

larger than the surface area of the TE modules (5 x 16 cm^2) in order to reduce the heat flux. As the ratio of the enhanced surface to the module surface increases further there are tradeoffs with the increase in thermal resistance of the material. Additionally, the heat transfer coefficient increases with heat flux, which will be discussed in Section 3.1.3.2.

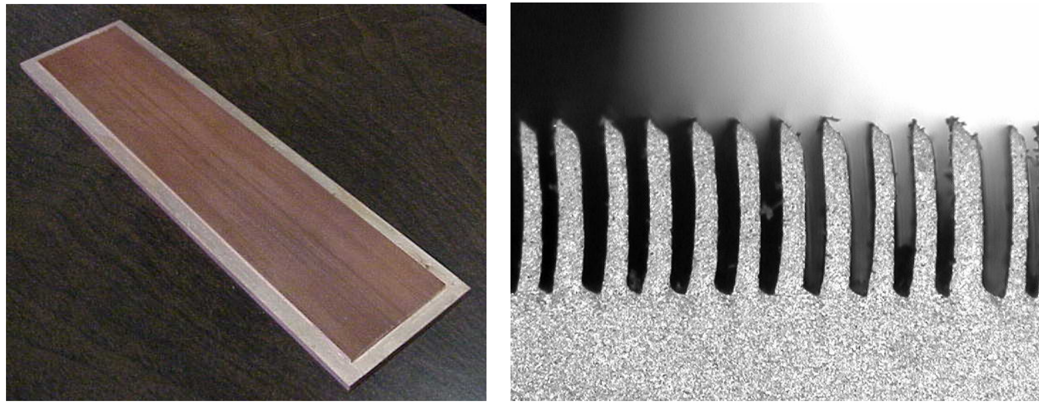

Figure 10: Micro Deformation Technology enhanced boiling surface from Wolverine Tube, Inc. for the third generation TE subcooler.

For each of the thermosyphon evaporators a copper cover plate was machined and brazed to the enhanced boiling surface. Inlet and outlet ports for the thermosyphon refrigerant were also machined. For the second generation subcooler, copper tubes were brazed to the cover plate. For the third generation subcooler, NPT threads were tapped to reduce the amount of brazing required.

The second generation thermosyphon was pressure tested with nitrogen in a water bath to 1950 kPa. Although the heat exchanger held the pressure, both the enhanced boiling surface and cover plate deformed. An attempt was made to squeeze the heat exchanger back into shape using a press. Unfortunately, some deformation remained. Due to safety concerns it was decided that machining the surface flat would remove too much material

and would compromise the safety of the heat exchanger. Similar to the microchannel a flat stone was used to sand the surface as flat as possible, with some success.

Because the copper heat exchanger was unable to hold the pressure without deformation it was necessary to change thermosyphon refrigerant. Initial testing on the first generation subcooler was performed with R22 as the thermosyphon refrigerant, which has a saturation pressure of 1360 kPa at 35°C. Subsequent testing was conducted using R134a, which has a saturation pressure of 890 kPa at the same temperature.

When constructing the third generation thermosyphon evaporator the sides of the cover plate were machined flat before brazing to the enhanced boiling surface. This was done to allow the joined evaporator to be put back into the mill to machine the outer surface flat. Unfortunately, due to warpage in the center of the enhanced boiling surface during brazing, a portion could not be machined flat. Tin-Silver solder was used to fill in the divot, and the entire surface was sanded flat.

2.1.5: Thermal Interface Material

As discussed previously, there exists a thermal contact resistance between the ceramic surfaces of the TE modules and the two heat exchangers. Thermal contact resistance arises due to surface roughness, which creates points of contact interspersed with air gaps. In order to limit this thermal resistance a thermal interface material (TIM) was used that fills the gaps caused by the surface roughness. The thermal resistance of the contact area with a TIM actually consists of three thermal resistances; the contact between the

TIM and the heat exchanger, the contact between the TIM and the TE module, and the thermal resistance across the layer of TIM. Predicting the total thermal resistance is a difficult task and was not a focus of this study. From this point forward the thermal resistance of the TIM material with a reduced thermal conductivity was assumed to equal the total thermal resistance of the contact area.

Initial construction of the second generation subcooler utilized Liquid Pro liquid metal thermal interface material. This Gallium based material, has a thermal conductivity of 82 W/mK, which is almost 10 times greater than Arctic Silver thermal grease. Unfortunately, the Liquid Pro did not bond with the ceramic surface of the TE module and therefore the thermal contact resistance was not improved. As a result Arctic Silver was chosen as the TIM for both the second and third generation subcooler for its ease of application and relatively high thermal conductivity of 8.9 W/mK compared to other thermal greases.

2.1.6: TE Subcooler Assembly

The assembly procedure for both the second and third generation subcoolers was identical. Once the surfaces of both heat exchangers were sanded as smooth as possible, all surfaces were cleaned thoroughly with acetone and again with alcohol with non-filament tissues. The surfaces of the heat exchangers were then coated with the TIM using a razor blade to spread the TIM as thin as possible. The five modules were placed on top of the coated surface of one heat exchanger and pressed firmly. The second heat exchanger was then placed on top of the modules. On the outside of each heat exchanger

was a 1/4th inch (6.35 mm) thick aluminum plate with pre-drilled holes for bolts. Once the assembled the bolts were put in place and tightened to supply an even pressure over each module. The modules were wired electrically in series with 12 gauge wire soldered to each of the electrical copper leads. Figure 11 shows a picture of the assembled third generation subcooler.

In order to characterize the performance of the second generation subcooler, temperature measurements of the hot and cold surfaces of the TE modules are needed. Before assembly, the stability of a TE module was checked with a thin thermocouple wire (0.075 mm diameter) in the TIM between the module and a flat copper plate. Unfortunately, even with the thin thermocouple wire, the modules teetered on the wire. As an alternative the wires were place in the gaps between the modules as shown in Figure 12.

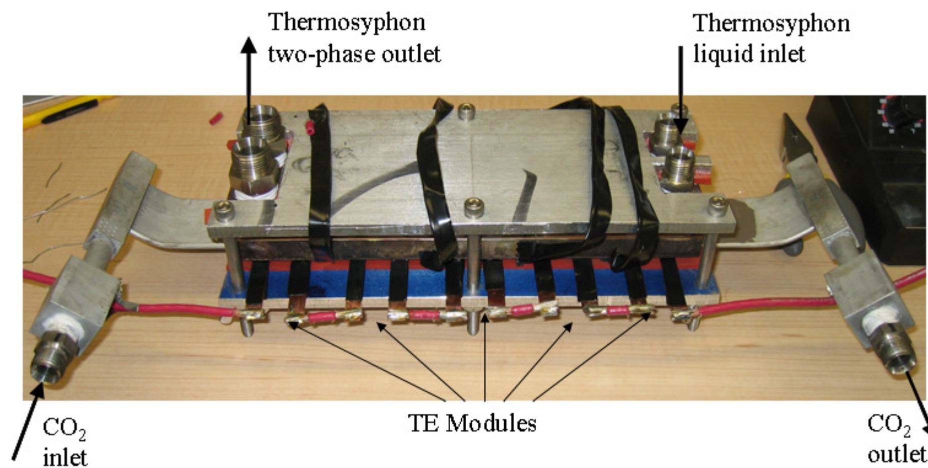

Figure 11: Third generation subcooler.

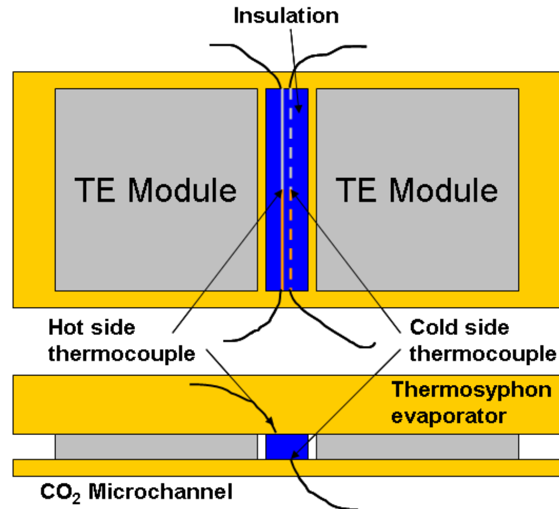

Figure 12: Diagram of the second generation subcooler with thermocouples.

The same assembly was used for the third generation subcooler, except only the hot side thermocouples were installed as the voltage measurements allow for a determination of the temperature difference across the module.

2.2: Experimental Setup

2.2.1: CO_2 System

A small CO_2 transcritical vapor compression cycle refrigeration system was built in order to experimentally verify the system performance improvements of a TE Subcooler. Figure 13 shows a schematic diagram of the experimental setup. The system was built with a prototype Danfoss CO_2 compressor. Previous testing on the compressor had shown a cooling capacity of roughly 1.4 kW at a suction pressure of 4.5 MPa.

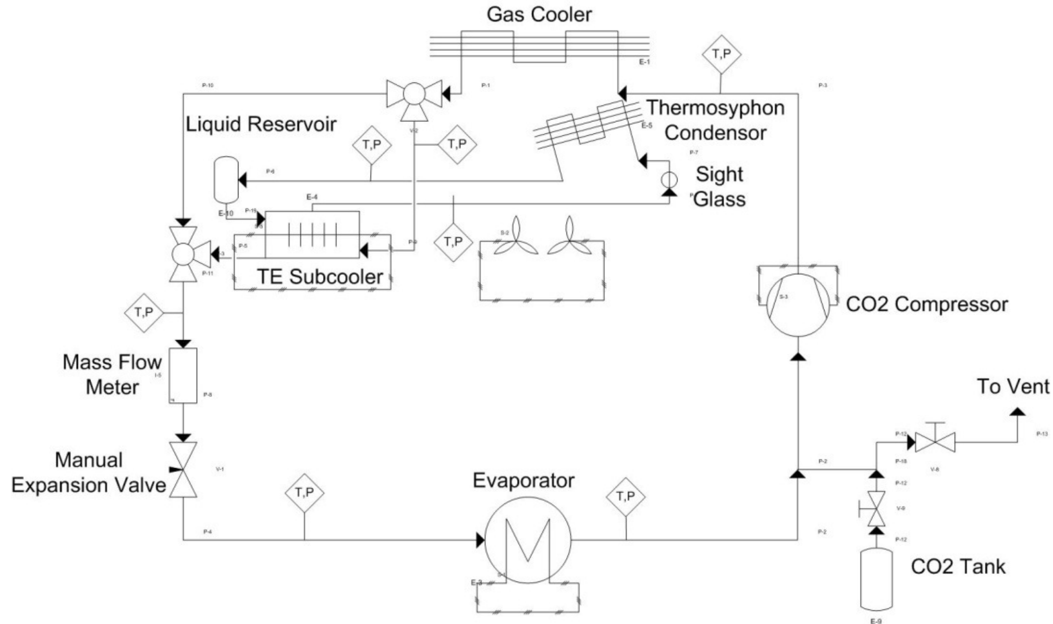

Figure 13: Schematic of the experimental setup

The gas cooler was assembled from two banks of two aluminum microchannel, louver-fin heat exchangers connected in series. Each of the four heat exchangers had 34, 19 mm wide microchannels spaced 1 cm apart with a fin density of 16 fpi. Each microchannel had eight 1.6 mm by 1.2 mm rectangular ports. A set of two automotive radiator fans were installed below the gas cooler. The CO_2 entered the top bank on the right and exited the bottom bank on the left. The gas cooler was assembled in this way to limit oil retention and to ensure the exiting CO_2 was exposed to the coolest air temperature to reduce the approach temperature. The CoilDesigner® simulation tool [30] was used to ensure the approach temperature was no greater than 5 K. The TE Subcooler was installed after the gas cooler and before the expansion valve.

A manual expansion valve was used as an expansion device. For the first round of testing a Swagelok SS-ORS2 Regulating stem valve was used. Subsequent tests were performed with a low flow Swagelok SS-31RS4 metering valve to give better pressure control.

The evaporator was constructed out of thick-walled 3/8” (9.525 mm) copper pipe wrapped in four separate heating tapes with a total heating capacity of about 2.0 kW. The pipe inner diameter was such that the mass flux remained above 300 kg/m^2s for mass flow rates above 10 g/s. According to Lee et al. (2003) [17] increased mass flux significantly reduces oil retention in the heat exchangers of CO_2 systems and results in a lower pressure drop penalty factor. The use of heating tape to simulate the cooling load simplified the system and allowed for a flexibly sized evaporator. The output of one of the heating tapes was controlled by a variable-voltage AC power supply.

The first round of testing was performed with the first generation subcooler aligned vertically, with CO_2 entering at the top from the gas cooler and exiting at the bottom to the expansion valve. The thermosyphon refrigerant, in this case R22, boiled within the heat rejection microchannels. The vapor refrigerant traveled upward to the thermosyphon condenser, where it condensed and traveled back to the inlet of the heat rejection microchannels at the bottom of the TE Subcooler. Figure 14 shows a picture of the setup for the first round of testing. An aluminum microchannel heat exchanger, the same as those used in the gas cooler, was used as the thermosyphon condenser. The vapor line exiting the thermosyphon evaporator was constructed out of copper pipe with a minimum inner diameter of ½ inch (12.7 mm) in order to reduce pressure drop. The vapor line was also insulated to reduce condensation on the walls of the pipe that would cause a counter-flow effect. Initially, the thermosyphon condenser was placed below the gas cooler on the inlet side, but above the fan. By configuring in this way, no additional fans were required

for the thermosyphon condenser. Subsequent testing was performed with the thermosyphon condenser removed from the gas cooler, requiring an additional fan.

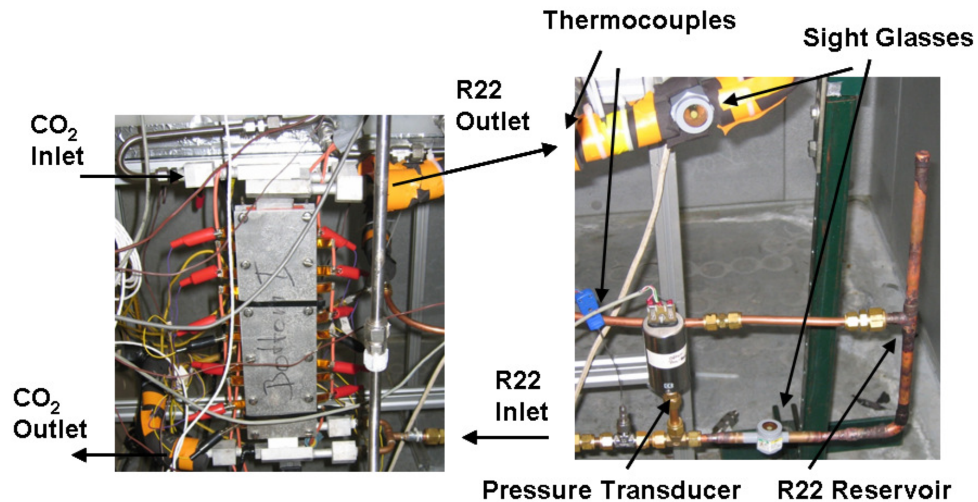

Figure 14: Round 1 TE Subcooler setup.

A refrigerant reservoir was utilized to hold additional liquid refrigerant in an effort to minimize the sensitivity of the thermosyphon performance to the refrigerant charge. Sight glasses were installed to assist in charging the thermosyphon loop by giving a view of the refrigerant liquid level.

The second round of testing was performed with both the first and second generation subcoolers installed in series on the CO_2 side and in parallel on the thermosyphon side. Both subcoolers were installed horizontally on a 10-15 degree angle to minimize the contact between the vaporized refrigerant and the boiling surface. An electrical cabinet was installed to allow for each subcooler to be tested independently or together as one large subcooler.

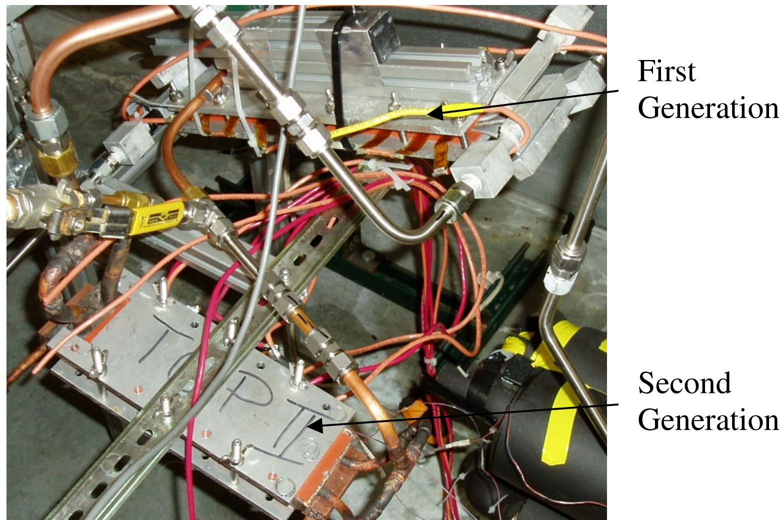

Figure 15: Testing rounds 2 and 3 TE Subcooler setup.

Finally, the third round of testing was performed with roughly the same setup as the second round with the first generation subcooler remaining and the second generation subcooler replaced by the third generation subcooler. The electrical cabinet was also used to allow each subcooler to operate individually or together. Figure 15 shows a picture of the second and third round setup.

2.2.2: Measurement and DAQ System

In order to characterize the system performance, in-stream Omega Engineering, Inc. T-type thermocouples and Setra capacitance pressure transducers were installed at the compressor suction and discharge, gas cooler outlet, TE Subcooler outlet, and evaporator inlet. In-stream T-type thermocouples were also installed in the refrigerant loop of the thermosyphon at the inlet and outlet of the TE Subcooler. An additional pressure sensor was also installed in the refrigerant loop. The mass flow rate (MFR) of CO_2 was measured by a Micro Motion R025P coriolis mass flow meter. Ohio Semitronics watt meters were installed to measure the power input to the compressor and the evaporator

heating tapes. A solid state relay was installed to shut off the compressor power in case of extreme discharge pressure. Additional T-type thermocouples were installed at the air inlet of the gas cooler fans. A constant current 200W HP 6033A System Power Supply with a digital display was used to power the thermoelectric modules. The voltage drop across each TE module was measured directly by the DAQ system. Measurement data was taken by a National Instruments FieldPoint® DAQ system controlled by an external computer running LabVIEW® [31].

The pressure transducers were calibrated using an Eaton Consolidated Controls pressure sensor over the entire pressure range of the system. Voltage readings were taken at several different pressures between 2 MPa and 10 MPa and a linear best fit was used to relate the voltage output to the pressure. The mass flow meter was calibrated using a liquid gravimetric method over a range from 0 to 20 g/s.

The system capacity, Q_{sys}, was calculated from the mass flow rate, $\dot{m}$, compressor suction enthalpy and evaporator inlet enthalpy as shown in Equation 10. Specific enthalpies, denoted by h, were determined from the temperature and pressure measurements using the NIST Refrigerant Database, REFPROP [32]. It was assumed that the expansion device was isenthalpic, so the enthalpy entering and exiting the expansion valve are equivalent. The system COP was calculated from the system capacity, compressor power input and, if used, the subcooler power input as shown in Equation 11. The power input to the fans was not considered in this analysis.

$$Q_{sys} = \dot{m}\left(h_{cmp,suct} - h_{evap,in}\right) \quad \textbf{(10)}$$

$$COP_{sys} = \frac{Q_{sys}}{P_{cmp} + I\sum V_i} \quad \textbf{(11)}$$

The TE Subcooler capacity was calculated in much the same way as the system capacity, except the enthalpies at the inlet and outlet were for the subcooler. The power input to the TE Subcooler was calculated as the product of the supply current, *I*, and the measured voltage drop across each module, V_i. The TE COP (COP_{TE}) was calculated using the Equation 12.

$$COP_{TE} = \frac{Q_{TE}}{I\sum V_i} \quad \textbf{(12)}$$

The uncertainties of the capacity and COP of the TE Subcooler are dominated by the uncertainty of the temperature measurements at the inlet and outlet. This is because of the large changes in enthalpy as a result of changes in temperature near the pseudocritical point. The in-stream T-type thermocouples have an uncertainty of ±0.5 K which resulted in large uncertainties during the first round of testing. In subsequent testing the T-type thermocouples at the outlet of the gas cooler and TE Subcoolers were replaced with RTD temperature probes which have an uncertainty of ±0.1 K. Table 1 gives the uncertainty for each of the measurement devices.

Both the CO_2 system and thermosyphon were checked for leaks and thoroughly evacuated before being charged with CO_2 and refrigerant, respectively. Testing was performed within an environmental chamber to maintain ambient temperature control. Steady state performance was measured over 20 minute intervals at a measurement frequency of 1 Hz. All tests were run at a constant superheating of 11.1 ±1.0 K according

to ANSI/ARI Standard 540 (1999) [20]. The compressor suction pressure and superheat were controlled by manual adjustment of the heating tape voltage and the expansion valve. The compressor discharge pressure was regulated by adjusting the CO_2 charge.

Table 1: Measurement device uncertainties.

Measurement Device	Uncertainty
T-type thermocouples	±0.5 K
RTD temperature sensor	±0.1 K
Pressure transducers (CO_2 system)	±23 kPa
Pressure transducer (Thermosyphon)	±2.3 kPa
Coriolis mass flow meter	±0.5 % of rate
Watt meters	±0.2 % of rate
TE Power Supply (current)	±0.15% of rate
DAQ (voltage)	±3mV + 0.3% of rate

2.2.3: Energy Balance

An energy balance was performed on the evaporator. The cooling capacity as calculated by Equation 10 was compared with the power input to the heating tapes as measured by the watt meters. The heating tapes were wrapped in two layers of insulation. The first was glass fiber insulation with a high temperature rating. The second was a layer of Armaflex insulation with a known thickness and thermal conductivity. Thermocouples were installed on the inside and outside of the second layer of insulation and the heat loss through the insulation was estimated from the temperature difference [19].

During the third round of testing, a larger than normal error in the energy balance was calculated. It was determined that the cause of the discrepancy was excessive oil circulation (OCR). This was confirmed by running a single test with the evaporator outlet temperature equal to the expansion valve inlet temperature, which minimizes any effect of oil on the energy balance. The test reported a near 0% error in energy balance. Suss

and Veje (2004) [13] reported on the development of the same compressor and reported an OCR of 5% at the test conditions under investigation in this study. Therefore the mass flow rate for the third round of testing was corrected for the OCR.

2.2.4: Test Matrix

Three TE Subcoolers were tested. Preliminary testing was performed on the first generation subcooler with the thermosyphon condenser integrated into the gas cooler. Subsequent testing was performed with the thermosyphon condenser removed from the gas cooler.

The first round of testing was performed on the first generation subcooler utilizing all ten thermoelectric modules. The ambient temperature of the chamber was set to 35°C and the suction pressure held constant at 4,198 kPa. This corresponds to a saturated vapor temperature of 7.2°C as recommended by ANSI/ARI Standard 540 (1999) [20]. As discussed above, the superheat was kept constant at 11.1 K. Testing was performed at compressor discharge pressures over the range required to show a maximum COP for the baseline and TE Subcooler systems. The supply current was increased from 0 Amps, in the baseline case, to the maximum value while maintaining a TE COP greater than the baseline system.

The second round of testing was performed on one side of the first generation subcooler with five modules and the second generation subcooler. The subcoolers were tested individually and combined. The suction pressure was reduced to 2,906 kPa (saturation

temperature of -6.7°C) to approximate low temperature cooling applications, resulting in a reduced baseline capacity and COP. Due the increased uncertainty of the enthalpy with temperature measurements around the pseudocritical point, the chamber temperature was reduced to 30°C for this round of testing. As in the first round of testing the discharge pressure and supply current were varied over the necessary ranges.

The third round of testing was conducted after moving the system to a new building and environmental chamber. Tests were run at a suction pressure of 4,198 kPa and a chamber temperature of 35°C. Both the first and third generation subcoolers were installed and tested individually and combined in series as in Round 2. As in all tests the discharge pressure and supply current were varied over the necessary ranges. Table 2 summarizes the test conditions for each round of testing.

Table 2: Test Matrix

Round	TE Subcooler	# of Modules	Thermosyphon Condenser	Ambient Temperature (°C)	Suction Pressure (kPa)	Discharge Pressure (kPa)	Supply Current (Amps)
Prelim.	1st	5	Integrated	35	4198	8400-9600	0, 3-6
1	1st	10	External	35	4198	8800-9400	0, 3-6
2	1st, 2nd	5, 10	External	30	2906	7900-8800	0, 3-8
3	1st, 3rd	5, 10	External	35	4198	8600-9600	0, 3-12

Chapter 3: Results and Discussion

3.1: Experimental Results

3.1.1: Preliminary Testing

As discussed previously the preliminary testing was performed with the thermosyphon condenser integrated into the gas cooler in a series configuration. The first generation subcooler was used with five of the ten TE modules energized. Suction pressure was kept at a constant 4,198 kPa. Figure 16 shows the system COP over a range of discharge pressures. There was only a marginal difference between the system COP with and without the TE Subcooler. The TE COP of the TE Subcooler was greater than the baseline COP for each case except for one. Figure 17 shows the TE COP for each supply current and discharge pressure.

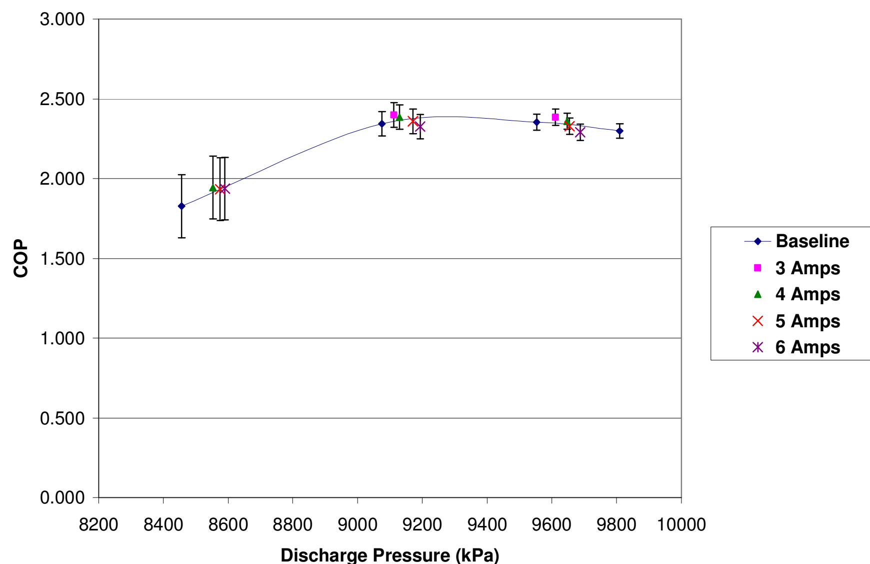

Figure 16: System COP for baseline system and with TE Subcooler at different supply current over a range of discharge pressures.

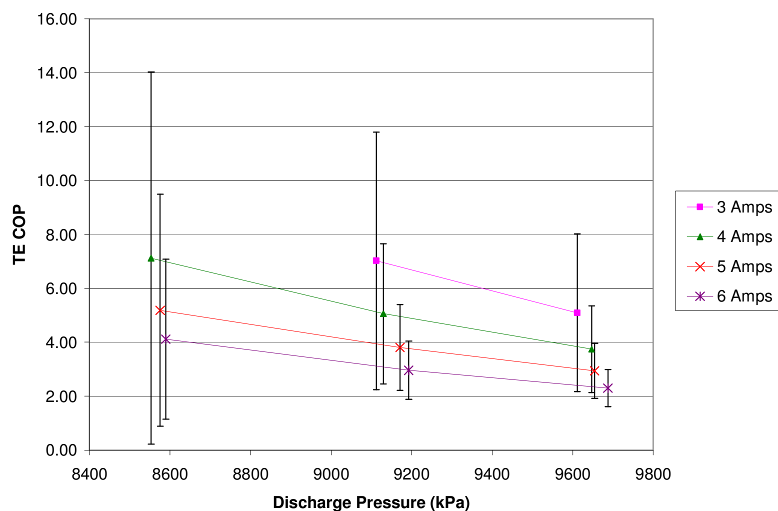

Figure 17: TE Subcooler COP at different supply current over a range of discharge pressures.

The reason the TE Subcooler did not have a positive impact on the system COP was the reduced capacity of the gas cooler as a result of the integrated thermosyphon condenser. Figure 18 shows the CO_2 gas cooler outlet temperature. As supply current is increased so is the heat rejection rate from the hot side of the modules and from the thermosyphon condenser, which drives the gas cooler outlet temperature up. It was for this reason that subsequent testing was performed with the thermosyphon condenser located outside the gas cooler assembly. This would be equivalent to a parallel configuration.

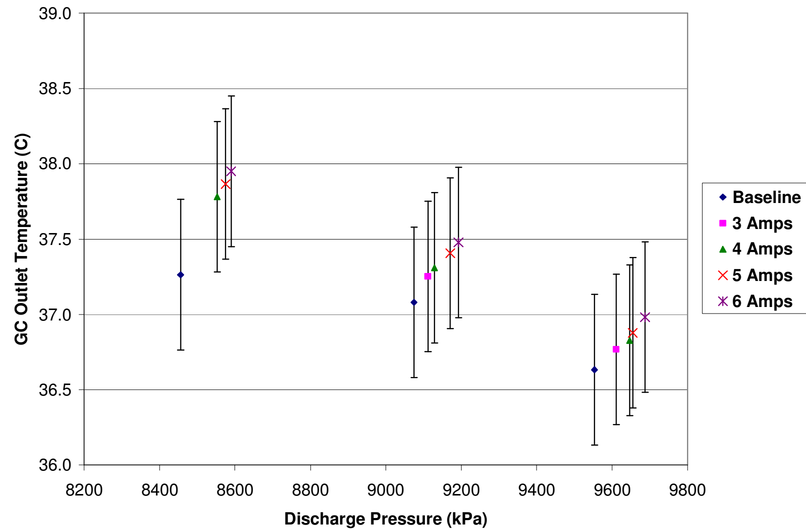

Figure 18: Gas Cooler (GC) outlet temperature for baseline and TE Subcooler system testing at different supply currents over a range of pressures.

3.1.2: First Generation Subcooler (Round 1)

3.1.2.1: System performance

The first generation TE Subcooler system was tested at a suction pressure of 4,198 kPa. The maximum COP for the baseline system was 2.35 at a discharge pressure of 9,553 kPa with a corresponding cooling capacity of 1.44 kW. The mass flow rate was 9.89 g/s. The measured approach temperature was 1.6 K, which was significantly less than the upper design specification of 5 K. Due to heat generated by the compressor and heating tape evaporator the gas cooler inlet air temperature was about ~0.8 K above the ambient temperature. With an approach temperature of less than a degree it is unlikely that increasing the gas cooler size would result in any significant system performance improvement. This is significant because the TE Subcooler requires additional heat exchanger area in the form of the thermosyphon condenser.

When employing the TE Subcooler a maximum COP of 2.48 was reached at a reduced discharge pressure of 9,042 kW with a corresponding cooling capacity of 1.57 kW. The maximum system capacity achieved utilizing the TE Subcooler was 1.66 kW at a COP of 2.38. The system performance for each of the three cases described above is listed in Table 3. For each of the TE Subcooler systems the CO_2 temperature entering the expansion device was below the ambient temperature of the chamber, resulting in capacity increases beyond what could be accomplished by increasing the size of the gas cooler.

Table 3: Baseline and TE Subcooler system performance at a suction pressure of 4,198 kPa.

	Baseline System (Maximum COP)	TE System (Maximum COP)	TE System (Maximum Capacity)
System COP	2.35	2.48 (+5.2%)	2.38 (+1.1%)
System Capacity (kW)	1.44	1.57 (+9.2%)	1.66 (+15.3%)
Discharge Pressure (kPa)	9,550	9,040	9,210
Compressor Power (kW)	0.610	0.591	0.601
Mass Flow Rate (g/s)	9.9	10.2	10.1
TE Supply Current (Amps)	-	4	6
Number of Modules	-	10	10
TE Capacity (kW)	-	0.204	0.256
TE COP	-	4.84	2.68
GC/TE Outlet Temperature (°C)	36.6	33.9	31.9

Figure 19 shows the system COP and capacity in response to discharge pressure. The discharge pressure varies slightly between the baseline and TE subcooler tests at different supply currents for a particular charge because of the degree of subcooling achieved. Subcooling increases the density of the CO_2, decreasing the pressure drop through the expansion valve. Since the evaporator pressure is kept constant, the high side pressure must be reduced.

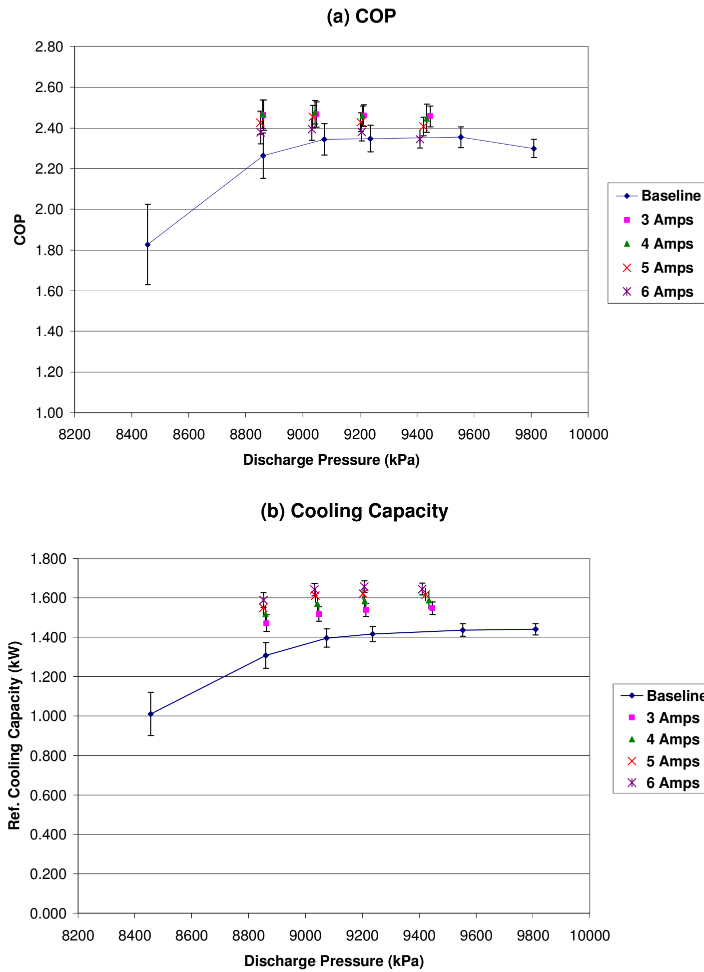

Figure 19: System performance response to discharge pressure.

The pressure-enthalpy (P-h) diagram for the baseline and TE Subcooler system with a maximum COP and the TE Subcooler system with a maximum capacity are shown in Figure 20. The increased slope during the compression process for the TE Subcooler systems reflects the increase in compressor efficiency at a reduced pressure ratio. For all cases the suction conditions were identical, which can be seen from the lower right point on the graph.

The increase in system capacity with the TE Subcooler is a result of two effects. First, by subcooling the CO_2 exiting the gas cooler the enthalpy entering the evaporator is reduced.

Since the suction enthalpy remains constant, the cooling capacity of the evaporator increases. Second, the increase in flow rate resulting from the increase in volumetric efficiency of the compressor also increases the available cooling capacity.

The system COP also increases as a result of two effects. First, since the TE modules operate at a COP greater than the baseline system the additional power required is proportionally less than the increased capacity. Additionally, there is a decrease in required compressor power input at a reduced pressure ratio.

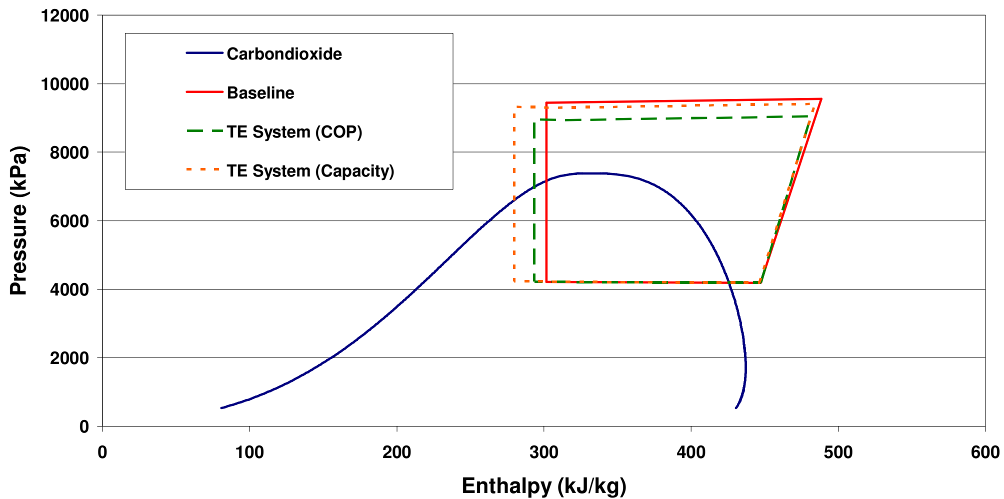

Figure 20: Pressure - enthalpy plot for the baseline system, TE System with maximum COP, and TE System with maximum capacity

3.1.2.2: TE Subcooler Performance

As the supply current is increased the increase in TE cooling capacity is offset by a greater increase in power consumption, reducing the TE COP. This occurs due to increases in joule heating and conduction from an increase in ΔT_m. This trend can be seen in Figure 21.

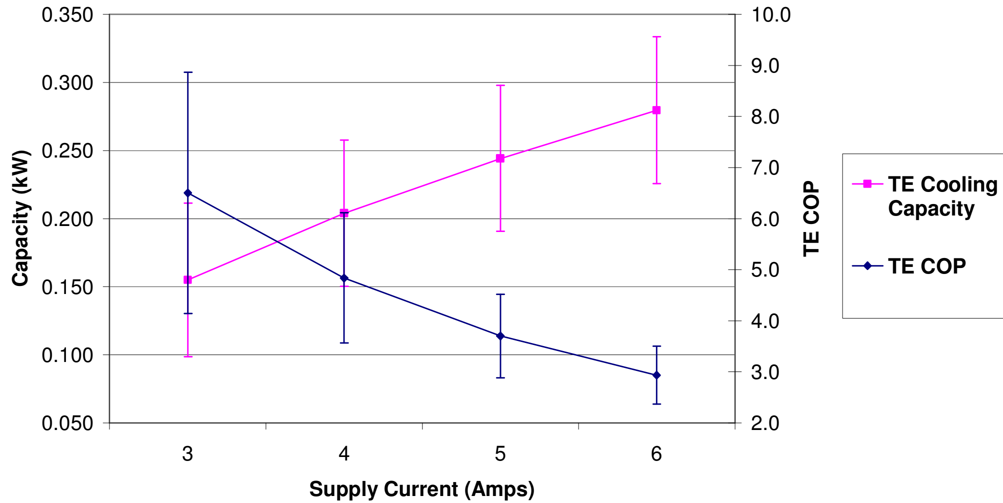

Figure 21: First Generation TE Subcooler performance at a compressor discharge pressure of ~9,040 kPa.

The increasing capacity of the TE Subcooler causes an increase in the temperature difference between the fluids by both decreasing the CO_2 temperature at the outlet of the subcooler as well as increasing the thermosyphon refrigerant temperature at the inlet of the evaporator as seen in Figure 22. The decrease in CO_2 temperature results is an unavoidable contribution to the ΔT_m.

The thermosyphon saturation pressure will increase if there is a greater rate of refrigerant boiling in the thermosyphon evaporator than condensing in the thermosyphon condenser. As the pressure rises, so does the saturation temperature until the condenser heat load is great enough to match the evaporation rate in the evaporator and equilibrium is reached.

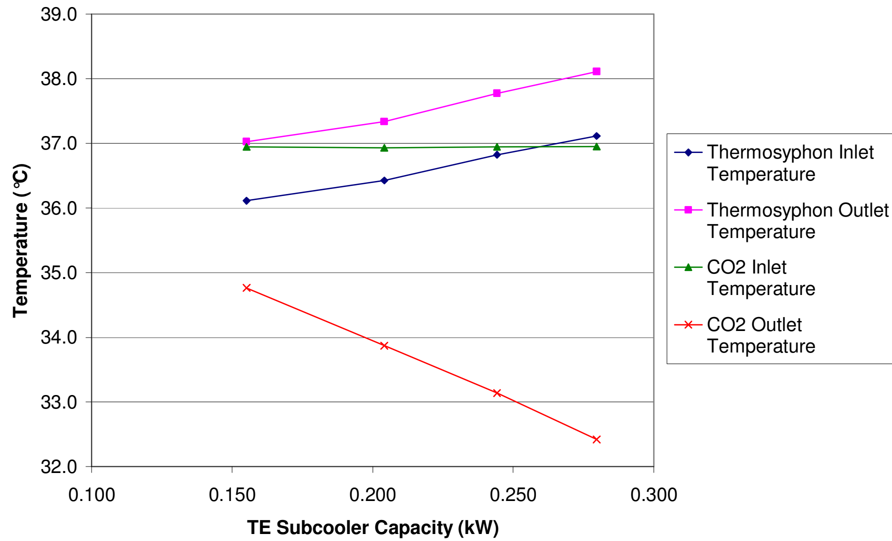

Figure 22: First Generation TE Subcooler fluid temperatures.

As seen in Figure 18 the gas cooler outlet temperature decreases as the discharge pressure is increased. This occurs regardless of the increased temperature at the compressor discharge. There are two reasons for this phenomenon. The first is the decrease in mass flow rate due to decreased volumetric efficiency with increased compressor pressure ratio. The second is the decrease in specific heat (C_p) with increasing pressure. Figure 23 shows the specific heat of supercritical CO_2 versus temperature for various pressures. There exists a peak C_p for each pressure at a particular temperature, known as the pseudocritical temperature. As the pressure increases the magnitude of the peak is reduced and the pseudocritical temperature increases. At low pressures the gas cooler is unable to reduce the temperature of the CO_2 below the pseudocritical temperature due to the location and magnitude of the peak C_p. At high pressures the same gas cooler will successful cool the CO_2 to temperatures below the peak C_p and because the mass flow rate and C_p are lower the approach temperature is reduced.

The decrease in gas cooler discharge temperature has a negative impact on the TE Subcooler performance as the module cold side temperature must be lower in order to pump heat from the CO_2 at a lower temperature. Additionally, the reduced mass flow rate and C_p at increased pressures causes the CO_2 within the TE Subcooler to decrease in temperature more rapidly, which leads to a greater reduction in the TE module performance toward the outlet.

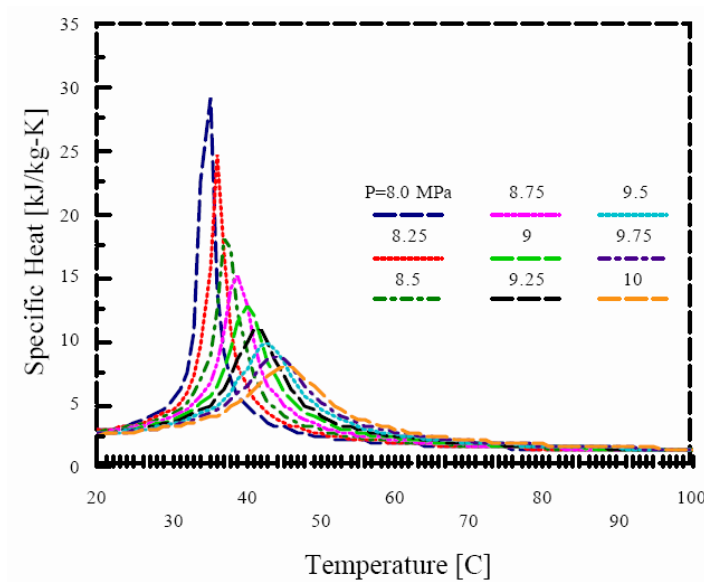

Figure 23: Specific heat of supercritical CO_2 versus temperature at various gas cooler pressures [22].

The decrease in mass flow rate has an additional negative effect on the TE Subcooler performance. As mass flow rate decreases so does the ratio of the inertial forces to viscous forces within the microchannel, also known as the Reynolds number. This causes an increase in the thickness of the viscous sublayer of the turbulent pipe flow, which represents the largest portion of the thermal resistance to convection with the microchannel wall. The heat transfer coefficient is therefore reduced at lower Reynolds number as can be seen from the Gnielinski correlation. Figure 24 illustrates the effects on TE Subcooler performance resulting from the increase in discharge pressure.

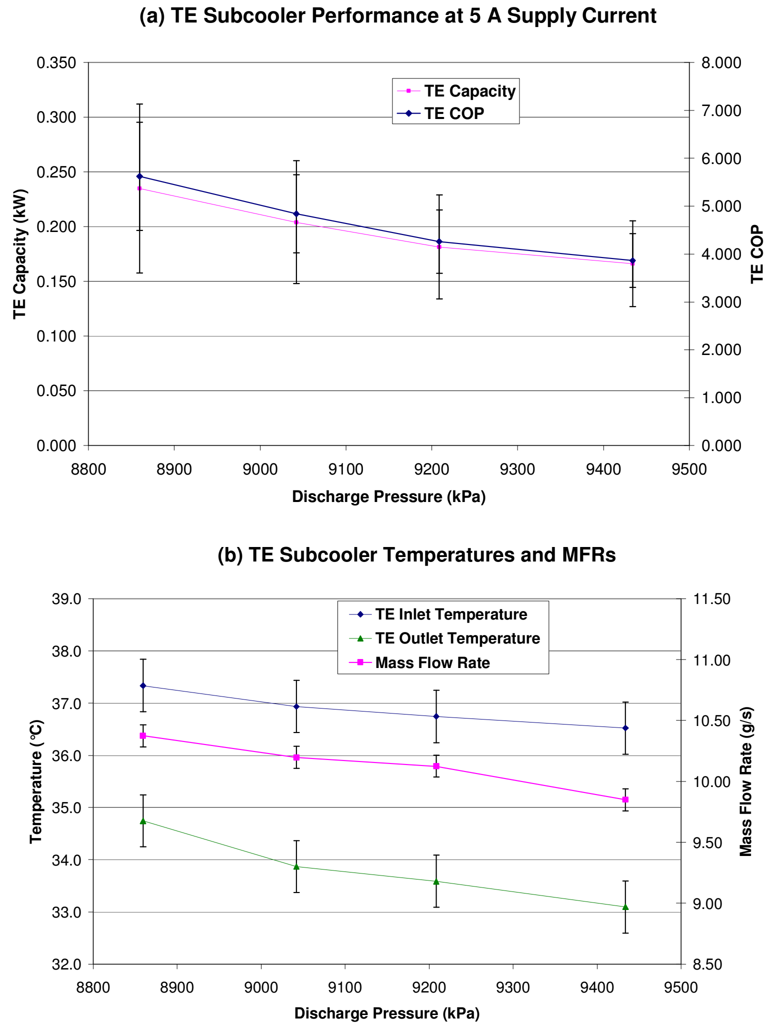

Figure 24: TE Subcooler performance dependence on discharge pressure.

3.1.3: First and Second Generation Subcooler (Round 2)

The second round of testing was performed on both the first and second generation TE Subcoolers at a suction pressure of 2,906 kPa. An electrical cabinet was constructed which allowed for either subcooler to be powered independently. As discussed previously, the chamber temperature was reduced to 30ºC. Since the gas cooler was already proven to be slightly oversized for the higher capacity case, the fan speed was reduced to give a more realistic approach temperature.

3.1.3.1: System Performance

The maximum system COP for the baseline system was 1.67 at a discharge pressure of 8,390 kPa. This corresponded to a capacity of 0.92 kW. The mass flow rate was 5.54 g/s. Even with the reduced gas cooler fan speed the approach temperature was below 1 K. The maximum COP achieved while utilizing the TE Subcooler was 1.80 at a discharge pressure of 7880kPa. The corresponding capacity was 1.04 kW. This was accomplished with the first generation subcooler. The maximum capacity achieved was 1.06 kW with a COP of 1.69 also at a discharge pressure of 7880. This was accomplished using both the first and second generation subcoolers in series. The temperature of the CO_2 entering the expansion valve for both TE Subcooler systems was lower than the ambient temperature. Table 4 shows the details of each of the systems described.

Table 4: System performance at a suction pressure of 2,906 kPa.

	Baseline System (Maximum COP)	TE System (Maximum COP)	TE System (Maximum Capacity)
System COP	1.67	1.80 (+8%)	1.69 (+1%)
System Capacity (kW)	0.92	1.04 (+12%)	1.06 (+15%)
Discharge Pressure (kPa)	8390	7880	7880
Compressor Power (kW)	0.552	0.531	0.531
Mass Flow Rate (g/s)	5.54	5.89	5.80
TE Subcooler	-	1st	1st & 2nd
TE Supply Current (Amps)	-	6	6
Number of Modules	-	5	10
TE Capacity (kW)	-	0.128	0.166
TE COP	-	2.84	1.76
GC/TE Outlet Temperature (°C)	30.7	27.7	26.1

As discussed previously, both the first and second generation subcoolers were installed in series into the system. They were tested separately and combined. Figure 25 shows the system COP for all testing completed during the second round. The legend on the right of

the figure gives the Subcooler, first or second generation, and the supply current in amperes. Figure 26 shows the system capacity using the same nomenclature.

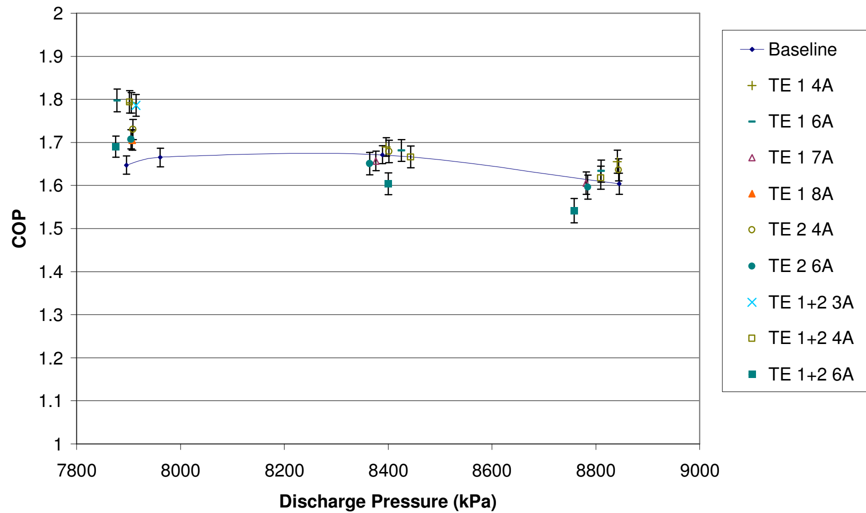

Figure 25: System COP for the baseline and TE Subcooler cases over a range of pressures.

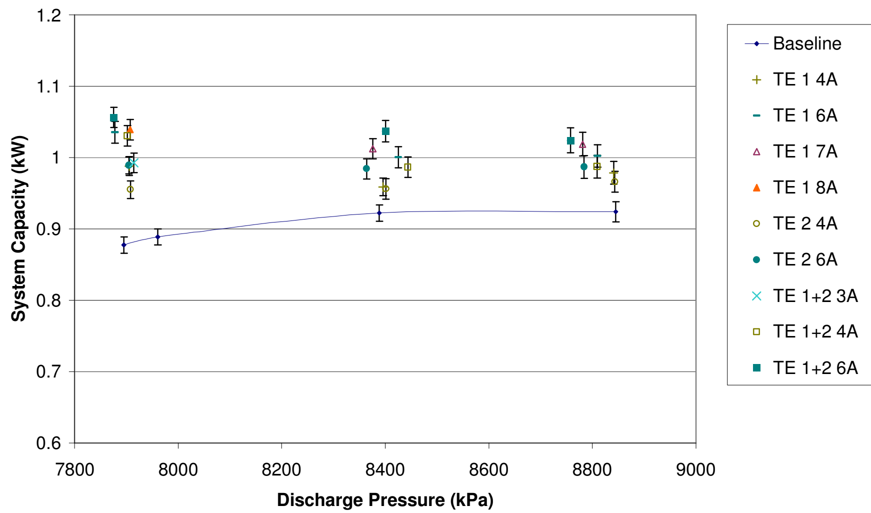

Figure 26: System capacity for the baseline and TE Subcooler systems.

As it can be seen in the figures, the greatest system COP and capacity is achieved at the lowest discharge pressure. Unfortunately, when the discharge pressure was reduced further it became difficult to reliably characterize the system due to large fluctuations in properties near the critical point. Therefore no data was taken at lower discharge

pressures. It may have been possible to achieve higher system COPs than those reported here, although it is unlikely due to significant reductions in the baseline COP at low discharge pressures.

3.1.3.2: TE Subcooler Performance

The performance of the first generation subcooler was superior to that of the second generation subcooler. Figure 27 shows the TE COP and TE capacity of the first, second and combined subcoolers at the lowest discharge pressure. When combined the total TE COP is reduced further due to the low CO_2 outlet temperatures achieved as shown in Table 4. The first generation subcooler was connected first in series and therefore operates at the same efficiency regardless of whether the second generation subcooler is powered. The second generation subcooler which was connected between the first generation subcooler and the expansion valve operates at a reduced TE COP due to the lower temperature CO_2 at the inlet.

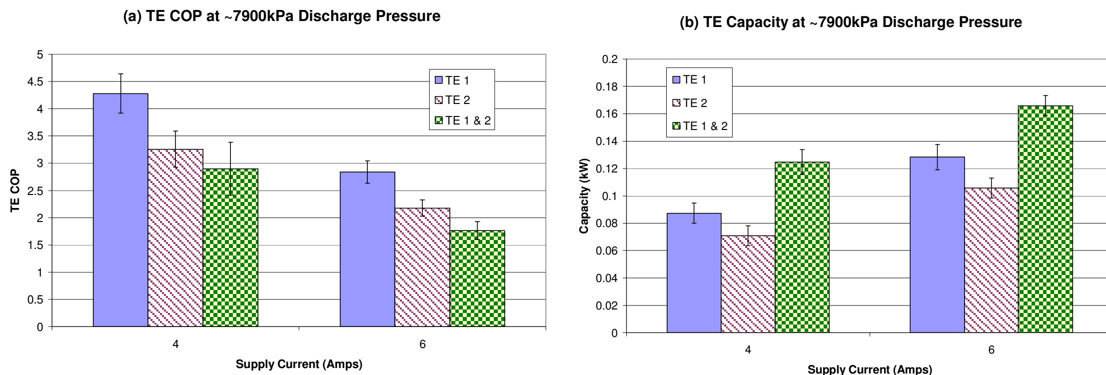

Figure 27: TE COP and Capacity for the first and second generation subcoolers for the low temperature cooling application at the low discharge pressure.

The preceding results demonstrate that the second generation subcooler did not perform as designed. The second generation subcooler was removed from the system and

disassembled in an effort to establish a root cause of failure. Figure 28 shows a picture of the TE module surfaces and the microchannel surface after separation. The dark area on the modules is the area that was in contact with the TIM. It can be seen that although TIM was applied to the entire microchannel surface, contact was not made over the entire surface. This was due to the fact that both the microchannel copper plate and the thermosyphon evaporator were extremely rigid but not perfectly flat. Even though the surfaces were squeezed together, an air gap still remained.

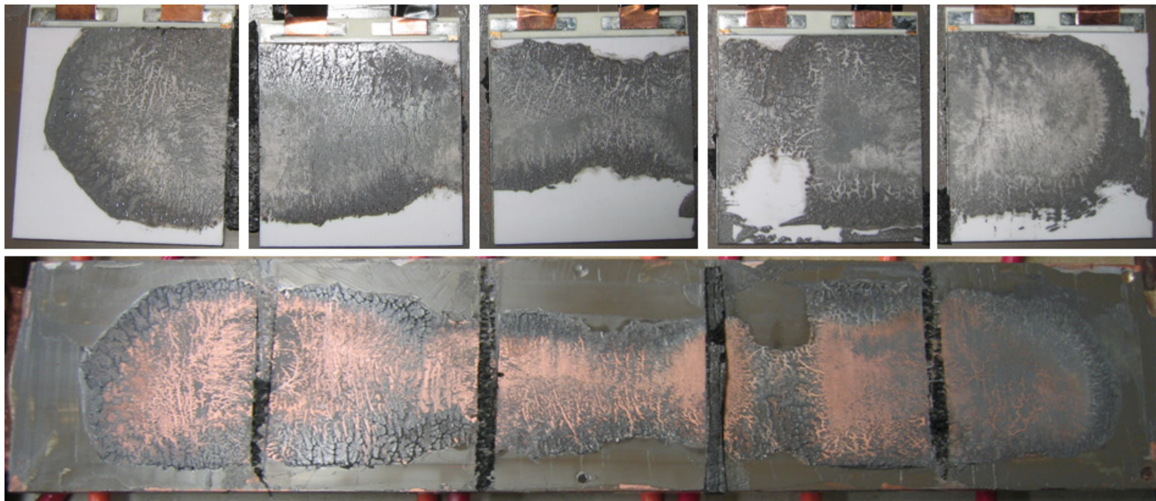

Figure 28: Module and heatexchanger surfaces after dissassembly of the Second Generation Subcooler.

An estimated 25% of the surface of the TE modules was not in contact with the microchannel heat exchanger. As a result, the ΔT across the thermoelectric couples in this area was greater than the maximum to pump any heat, resulting in greatly reduced module cooling capacity. The voltage drop across each couple with a ΔT greater than the maximum is also larger than if the ΔT is low enough to pump heat. This can be seen in Figure 29. As a result the total voltage drop and power consumption of the modules was increased. The expected voltage drop should increase over the length of the subcooler as

the ΔT_m across the module increases. This was the case for the first generation subcooler as seen from modules 1 through 5, but not for the second generation subcooler (modules 6 – 10). The voltage drop instead, was determined by the TIM coverage as shown in Figure 28. The highest voltage drop was in the first and third modules of the second generation subcooler because they have the least TIM coverage.

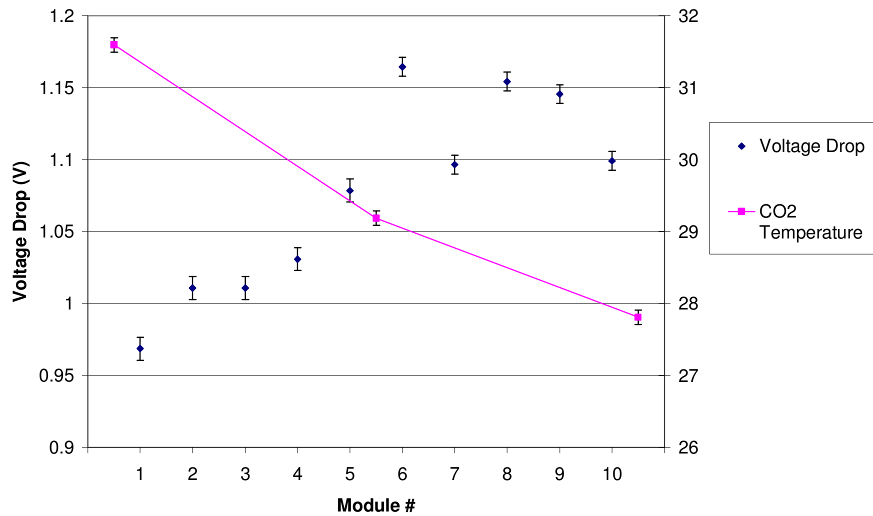

Figure 29: Voltage drop for each module along both the first and second generation subcoolers connected in parallel with a supply current of 4 amperes.

Figure 30 shows the temperature profile across the second generation subcooler at a supply current of 6 amps and a discharge pressure of ~7,900 kPa. The modeling techniques described in Section 2.1.2 were used to estimate the effectiveness of the subcooler with complete TIM coverage at a constant thickness. The temperature difference across each module was estimated from the measurements of the thermocouple within the second generation subcooler at a supply current of 6 amperes and a discharge pressure of ~7,900 kPa. The modules were assumed to pump only 75% of their theoretical capacity at the given ΔT. The other 25% of the modules was assumed to pump no heat with a corresponding increased voltage drop. The calculated total cooling

capacity was compared to the measured cooling capacity of 106 watts. A constant adjustment was made to each ΔT_m in order to minimize the error between the calculated and measured total cooling capacity.

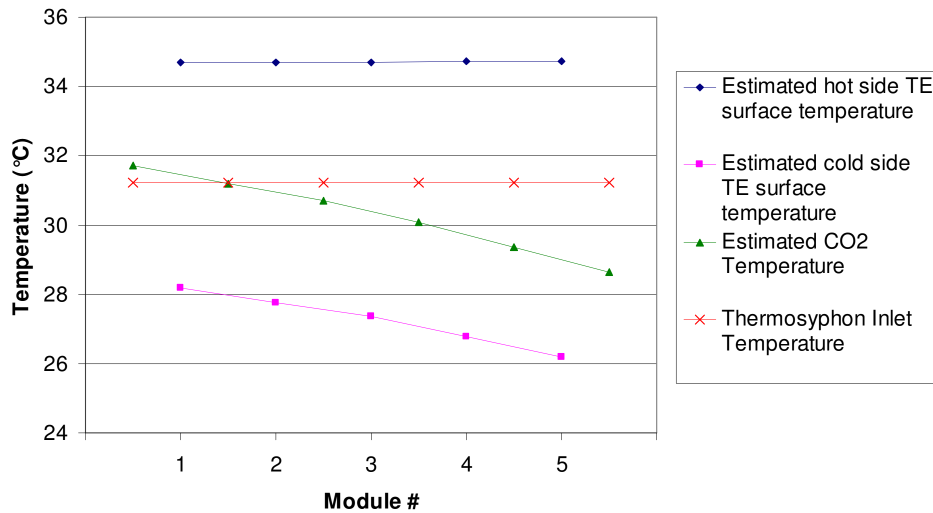

Figure 30: Temperature profile across second generation subcooler at 6 A and ~7900 kPa discharge pressure.

By decreasing the measured ΔT_m for each module by only 0.2 K the calculated capacity becomes 106 W. The calculated COP was 1.98, 9% lower than the measured COP of 2.18 ± 0.15. The thermal resistances were calculated for each module. To calculate the subcooler performance with full TIM coverage, the thermal resistance was decreased by 25% to account for the larger area. The CO_2 inlet temperature and pressure as well as the pressure drop were taken from the experimental conditions. The CO_2 temperature at each module was calculated from the Equations 4 – 6. The total calculated cooling capacity and TE COP were 139 W and 2.95, respectively. At the same supply current the first generation subcooler provided a cooling capacity of 128 ±9 W at a TE COP of 2.84 ±0.21. The difference between the calculated performance of the second generation

subcooler with full TIM coverage and the measured performance of the first generation subcooler was minimal. As shown in Table 4, the first generation subcooler with a supply current of 6 A resulted in the greatest performance improvement for the system.

It is now possible to look at the performance of the individual modules along the subcooler. Using the theoretical subcooler described above the cooling capacity and TE COP for each module was plotted as shown in Figure 31. Both the COP and capacity drop off sharply over the length of the subcooler. The trend suggests that if the subcooler had an additional module, it would operate at TE COP below the baseline system COP. This suggests that the subcooler was appropriately sized for the system as this estimated performance is representative of the subcooler performance which resulted in the greatest system COP increase.

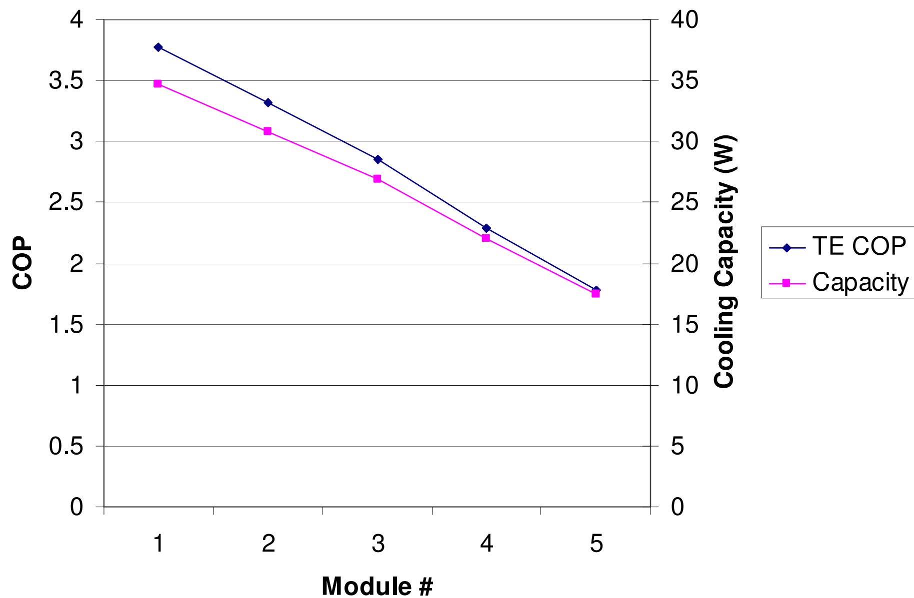

Figure 31: Estimated module performance over the TE subcooler.

The large decrease in performance can partly be attributed to the decrease in CO_2 temperature leading to an increase in ΔT_m across the modules at the end of the subcooler. Additionally, there are large changes in the CO_2 properties in the supercritical region that adversely affect heat transfer. As temperature decreases in the subcooling process the viscosity of the CO_2 increases. Similar to the reduction in mass flow rate as discussed in Section 3.1.2.2, increased viscosity causes a decrease in the Reynolds number and therefore a decrease in the heat transfer coefficient. Additionally, the specific heat also decreases. This causes a reduction in the ratio between the viscous diffusivity and the thermal diffusivity, also known as the Prandtl number. In turbulent pipe flow, reduced Prandtl number results in less radial thermal diffusion. The temperature profile becomes more rounded and convective heat transfer from the pipe wall is reduced. The temperature effects on conventional refrigerants in the subcooled region are marginal compared to supercritical CO_2. Figure 32 shows the decrease in Reynolds number and Prandtl number across the TE Subcooler discussed above.

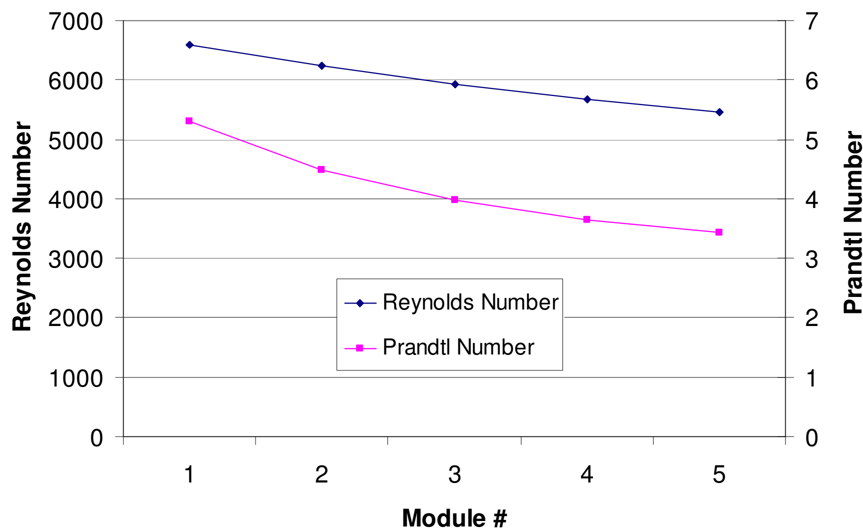

Figure 32: Calculated Reynolds and Prandtl numbers at each module of the TE Subcooler.

As discussed in Section 2.1.1 there are five thermal resistances within the subcooler, each of which have an associated ΔT that contribute to the ΔT_m. Using the same example case as above, the ΔT associated with each has been estimated using Equations 5 and 8. The brazing alloy used in the microchannel of the second generation subcooler constituted an additional thermal resistance. Table 5 shows the assumptions used to calculate each thermal resistance. The Mostinisk correlation [33] is a fairly accurate predictor of nucleate boiling based on the reduced pressure of the fluid, and is independent of the surface geometry. The HTC calculated from the Mostinski correlation was multiplied by a factor of 2.5 to account for the increased surface area of the enhanced boiling surface. The total ΔT_m calculated from the thermal resistances compared very well with the predicted ΔT_m from the analysis above, with largest difference less than 0.5 K.

Table 5: Parameter assumptions for ΔT calculation.

Parameter	CO_2 Side	Thermosyphon Side
TIM Thickness (mm)	0.25	0.25
TIM Conductivity (W/mK)	8	8
Copper Thickness (mm)	3.6	5
Copper Conductivity (W/mK)	401.2	401.2
Brazing Alloy Thickness (mm)	0.9	-
Brazing Alloy (W/mK)	110	-
HTC Correlation	Gnielinski	Mostinski

Figure 33 shows each of the contributing ΔT over the length of the subcooler. The greatest contributors are the convective heat transfer to the CO_2 and the pool boiling of the thermosyphon refrigerant. The decrease in microchannel convection ΔT is a result of the decreased heat flux at the end of the subcooler. The difference in fluid temperatures becomes a significant factor at this point as well. The material contributions on both sides are minimal. The TIM ΔT was between 1 – 1.5 K over the length of the subcooler.

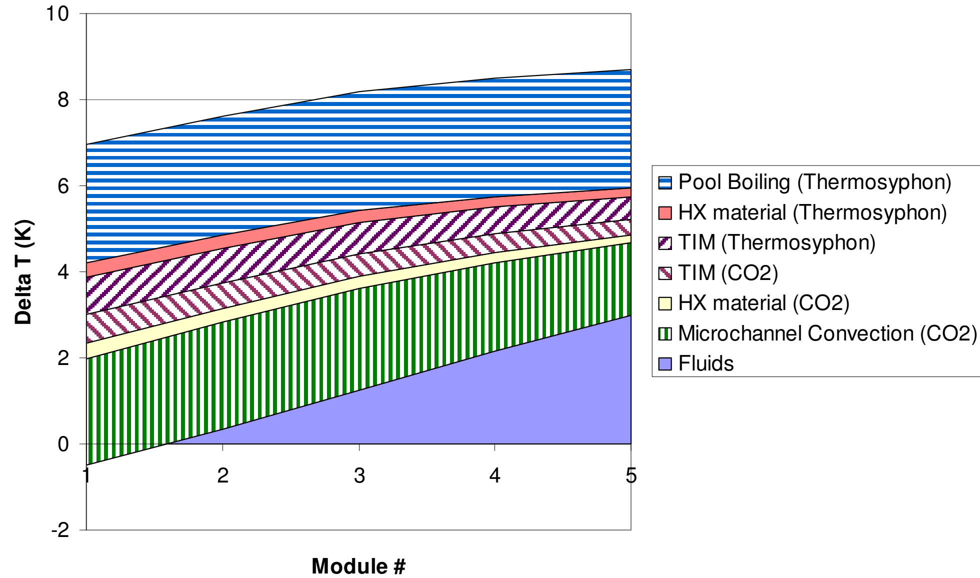

Figure 33: Contributing temperature differences across the TE Subcooler.

3.1.3: First and Third Generation Subcooler (Round 3)

3.1.3.1: System Performance

The final round of testing was performed on the first and third generation subcooler at a suction pressure of 4,198 kPa. Each subcooler was tested individually and combined in order to achieve the greatest system COP. Prior to testing, the system was moved to a new environmental chamber in a different building at the University of Maryland, resulting in a slight difference in line voltages and chamber air flow rates compared to the first round of testing. This resulted in a slightly different baseline performance than the first round of testing. The baseline system had a maximum COP of 2.38 with a corresponding capacity of 1.46 kW. Table 6 gives the key parameters from the baseline test and four different TE Subcooler tests. A maximum system COP of 2.62 with a corresponding capacity of 1.65 kW was attained utilizing both the first and third generation subcooler in series.

Figure 34 and 35 give the system COP and capacity at the three discharge pressures tested. The baseline system performance is significantly lower at the lowest discharge pressure, but with the TE Subcooler, system COP and capacity can match that of the optimum baseline system.

Table 6: System performance during third round of testing.

	Baseline (Max COP)	TE 3 System (Max COP)	TE 3 System (Max Capacity)	TE 1+3 System (Max COP)	TE 1+3 System (Max Capacity)
System COP	2.38	2.55 (+7%)	2.41 (+1%)	2.62 (+10%)	2.41 (+1%)
System Capacity (kW)	1.46	1.60 (+10%)	1.77 (+21%)	1.65 (+13%)	1.81 (+24%)
Discharge Pressure (kPa)	9270	9220	9240	9240	9210
Compressor Power (kW)	0.611	.609	0.612	0.609	0.608
Mass Flow Rate (g/s)	10.76	10.66	10.68	10.81	10.86
TE Supply Current (Amps)	-	4	10	3	7.5
Number of Modules	-	5	5	10	10
TE Capacity (kW)	-	0.164	0.340	0.179	0.381
TE COP	-	8.51	2.78	8.66	2.62
GC/TE Outlet Temperature (°C)	37.4	34.8	31.6	34.3	30.7

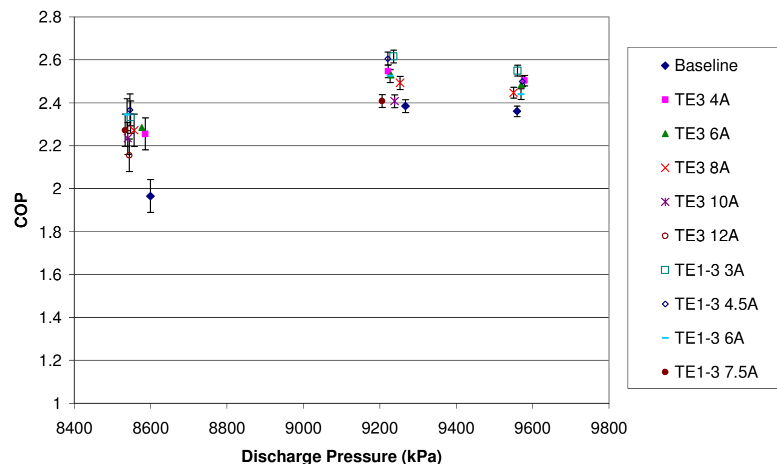

Figure 34: System COP for the third round of testing.

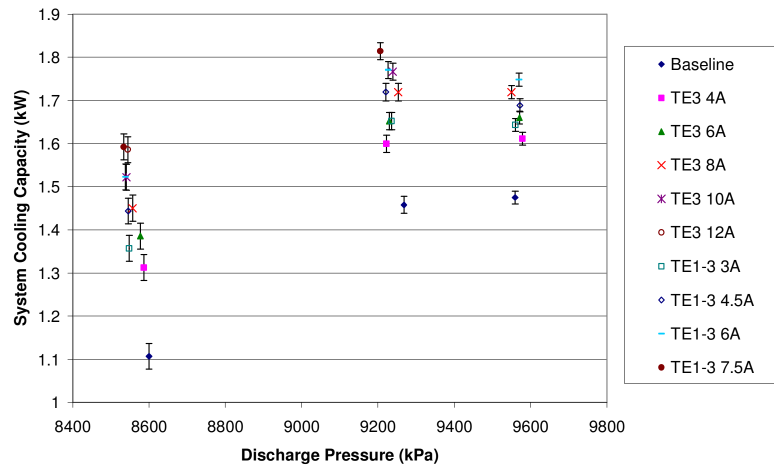

Figure 35: System capacity for the third round of testing.

The P-h diagram for the baseline system, TE Subcooler system with the maximum system COP and the maximum capacity are shown in Figure 36.

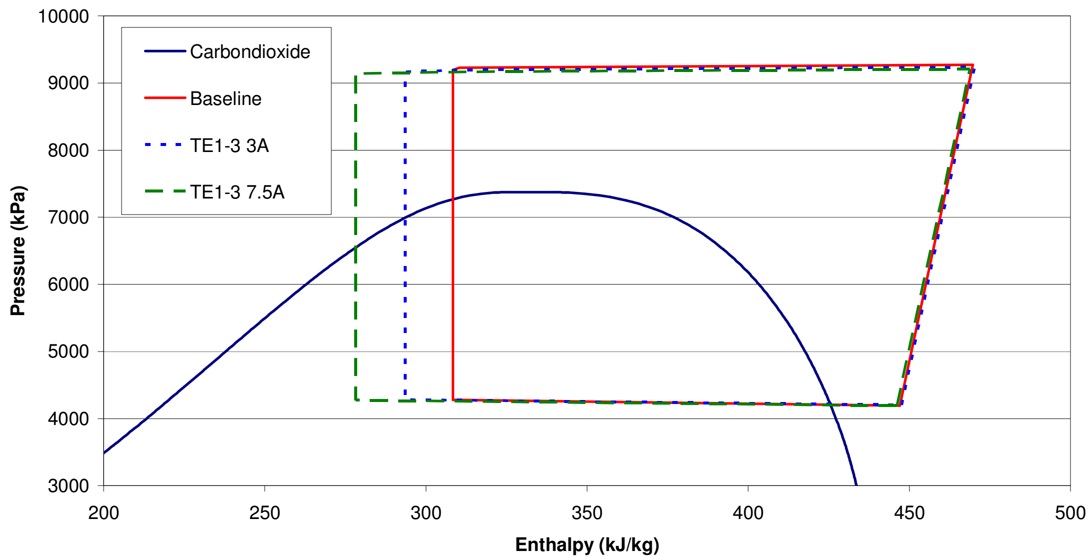

Figure 36: Pressure - enthalpy plot for the baseline system and combined 1st and 3rd generation TE Subcoolers at supply currents of 3A and 7.5A.

3.1.3.2: TE Subcooler Performance

The third generation subcooler outperformed the first generation subcooler at all pressures and supply currents. Figure 37 shows the TE COP and capacity of each

subcooler at discharge pressure of 9,200 kPa and a supply current of 4 A. Since both subcoolers utilized the same aluminum microchannel CO_2 heat exchanger the, thermosyphon evaporator of the third generation subcooler was likely to have a reduced thermal resistance compared to the microchannel evaporator used in the first generation subcooler.

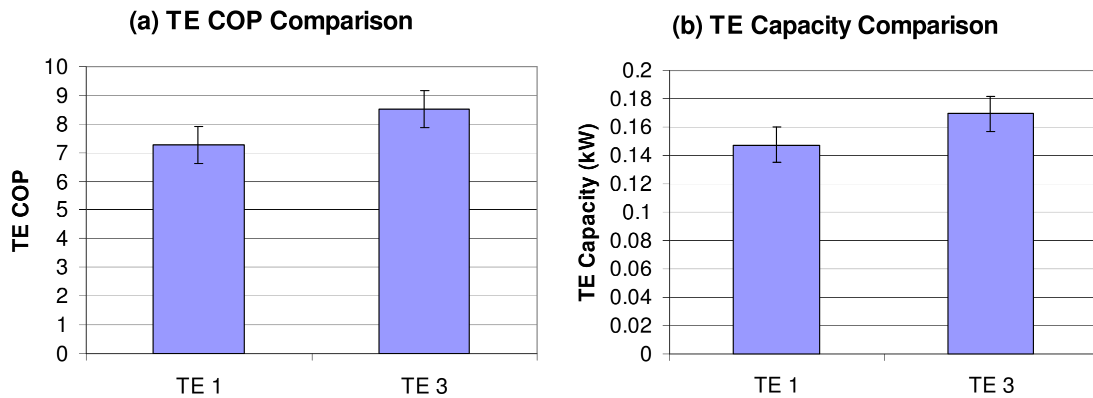

Figure 37: Performance of the first and third generation subcooler at a discharge pressure of 9200 kPa and a supply current of 4 Amps. a) TE COP b) TE Capacity.

As discussed previously, as the current is increased the capacity of the TE Subcooler increases and the COP decreases. Figure 38 shows the TE COP and capacity for the third generation subcooler and the first and third generation subcoolers combined at a discharge pressure of 9,200kPa. At higher supply currents the TE COP becomes lower than the baseline COP and therefore does not improve upon the performance of the system. The TE COP decrease is due to the increased joule heating effect as well an increase in the heat conducted through the thermoelectric elements at increased ΔT_m. The thermosyphon must remove the heat effectively from the hot side of the modules in order to minimize the hot side surface temperature and ΔT_m.

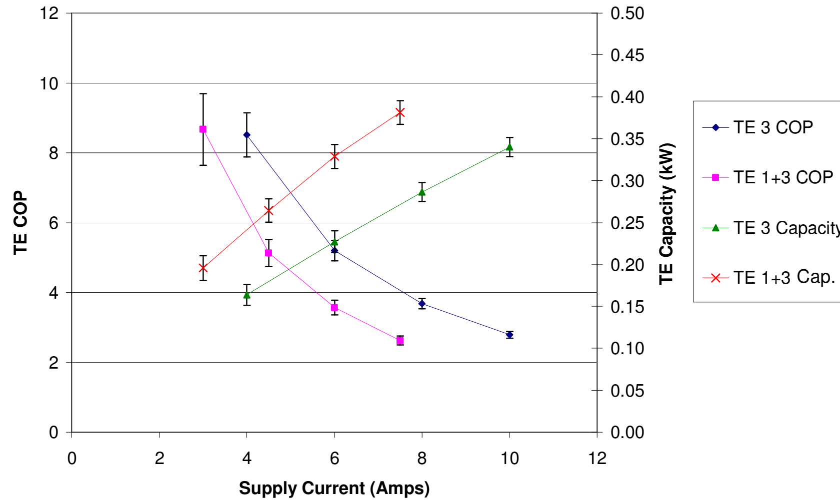

Figure 38: Third generation and combined first and third generation subcooler performance versus supply current.

The thermal resistances of the thermosyphon evaporator and thermosyphon condenser are defined using Equation 13 and 14. Figure 39 shows the thermal resistance of each component of the thermosyphon. Although there is some scatter due to fluctuations in temperature measurements, it can be seen that the total thermal resistance of the thermosyphon decreases with increasing heat rejection rate. This is due primarily to the decrease in thermal resistance of the evaporator with increased heat flux. This phenomenon has been well documented for enhanced boiling surfaces (Yuan, 2003 [23]) and confirms the presence of pool boiling. There are a number of different factors which account for the increase in the heat transfer coefficient with increased heat flux. Increased heat flux causes an increase in the bubble departure frequency which increases the rate of the liquid refrigerant pumped into the cavities between the fins to take the place of the departing vapor. This increase in flow rate causes an increase in the convection to the liquid refrigerant. At a high enough heat flux, only a liquid refrigerant film remains over portions of the enhanced surface. The presence of film boiling results in a further increase of the heat transfer coefficient. Finally, as discussed in Section 3.1.2.2 increased heat

rejection rates cause an increase in the saturation pressure of the thermosyphon refrigerant. The pool boiling heat transfer coefficient will also rise with increased pressure as the required nucleation superheat is reduced.

$$R_{evap} = \frac{T_H - T_{evap,in}}{Q_H} \quad \textbf{(13)}$$

$$R_{cond} = \frac{T_{evap,in} - T_{amb}}{Q_H} \quad \textbf{(14)}$$

Once the heat flux of the evaporator reaches roughly 42 kW/m^2 the thermal resistance flattens out and appears to increase, but more data at an elevated heat flux is necessary to confirm this trend. If the thermal resistance is increasing it could be due to dryout conditions on the enhanced boiling surface, in which the area between the fins is dry and the surface boils similar to a flat plate. Visualization is needed in order to determine this conclusively. It may be possible to optimize the microfin density in order to increase the heat flux at which dryout occurs.

Another factor which affects dryout is the refrigerant charge in the thermosyphon. If over charged, the thermosyphon will operate poorly at low heat rates. This is due to low vapor fractions within the vapor line causing a large pressure drop due to gravity. If under charged, the thermosyphon will operate poorly at high heat rates. This is due to a reduction in the driving force of the liquid head in the liquid return line. Compounding this problem is a further reduction of the liquid head at increased pressure due to the decrease in liquid density [24]. A low driving force may have caused the premature dryout conditions to occur in the thermosyphon evaporator. When attempting to optimize

the charge of the thermosyphon the TE Subcooler was set to a medium to low supply current which may have caused the thermosyphon to under perform at high heat rates.

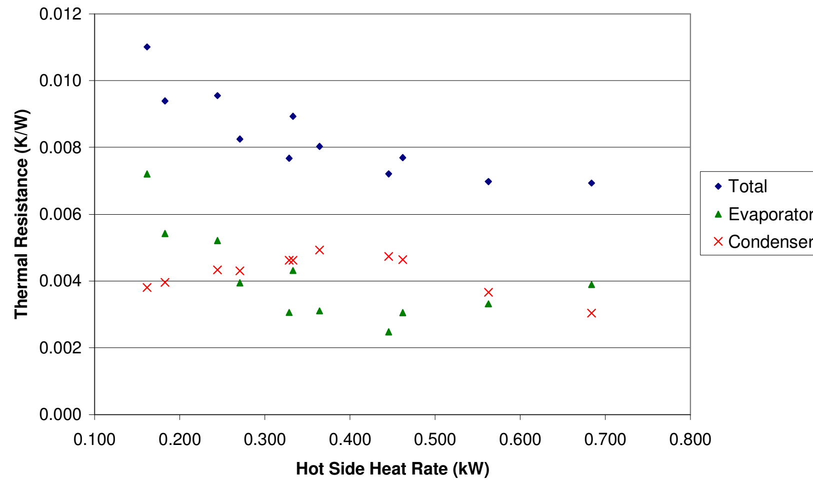

Figure 39: Thermosyphon thermal resistance versus heat rejection rate.

The condenser thermal resistance seems to increase slightly until a heat rate of approximately 380 W, at which point it begins to decrease. Ideally, the condenser thermal resistance should decrease with increasing heat rate due to an increased flow rate of refrigerant. A flow rate increase causes an increase in the shear stress on the condensate film on the inner wall of the channels, decreasing film thickness and increasing heat transfer [25]. It is possible that at low heat rates the vapor refrigerant flow is slower than the condensate film flow driven only by gravity and therefore does not reduce the film thickness. At a critical heat rate the vapor flowrate will surpass the liquid film flowrate and the increased shear stress will cause a decreased film thickness.

By operating both subcoolers simultaneously, it was possible to improve the system COP by a greater margin than either of the subcoolers individually. With 10 modules instead of five the supply current can be reduced, which increases the TE COP. Figure 40 shows

the voltage drop across each module. Modules 1 – 5 are from the first generation subcooler and modules 6 – 10 are from the third generation subcooler. The temperature at the inlet and outlet of each subcooler is also plotted in Figure 40. There is a general trend of increasing voltage drop as the CO_2 temperature is reduced. The voltages that don't follow this trend, specifically module 8, are higher due to the increased thermal resistance of the SnAg solder used in the thermosyphon evaporator. The voltage drop increase is not continuous from one TE Subcooler to the other. All the modules of the third generation subcooler have a lower voltage drop than the last module of the first generation subcooler. If the third generation subcooler had 10 modules the TE Subcooler and system performance would be improved.

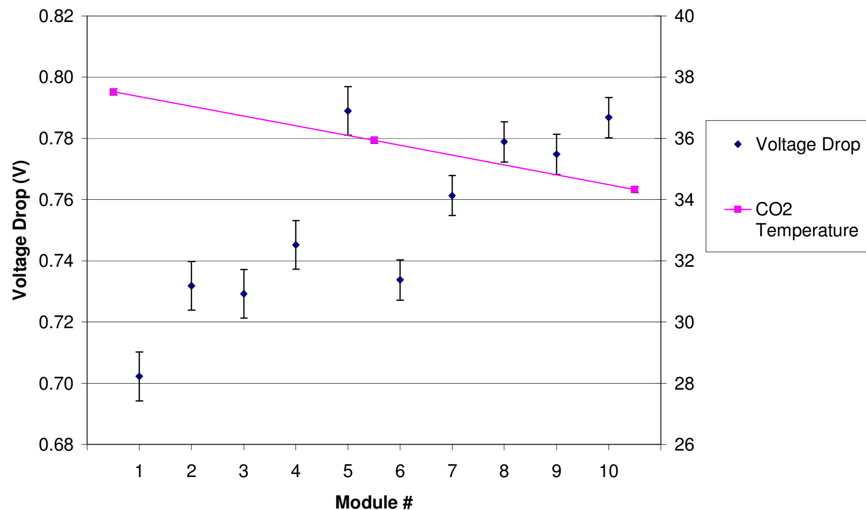

Figure 40: Module voltage drop and CO_2 temperature.

The ΔT_m was estimated from the voltage drop and the hot side surface temperature of the modules of the third generation subcooler at a supply current of 4 Amps and a discharge pressure of 9,200 kPa. In order to improve upon the accuracy of the prediction a new TE model was developed using equations 1 – 3. The temperature dependent properties were

evaluated from relations given in Xuan et al. (2002) [5] for Bismuth Telluride. The properties were adjusted in order to match the performance at a hot side surface temperature of 50°C and 85°C as given by the manufacturer of the TE modules. A slight increase in conductivity was made to account for the inclusion of radiation and convection heat transfer and a slight decrease in the Seebeck coefficient was made to account for the non-ideal performance of the Bismuth Telluride semiconductor. The adjustment factors are similar to those used in Nabi and Asias (2005) [2]. The total cooling capacity and TE COP were predicted to within 3% of the measured values.

Figure 41 gives the estimated hot and cold side temperature as well as the CO_2 temperature at each module. As seen in the analysis of the Round 2 results, the ΔT_m increases along the length of the subcooler. The TE COP and capacity also decrease with each module as shown in Figure 42, but the TE COP of the last module is still significantly higher than the baseline system COP.

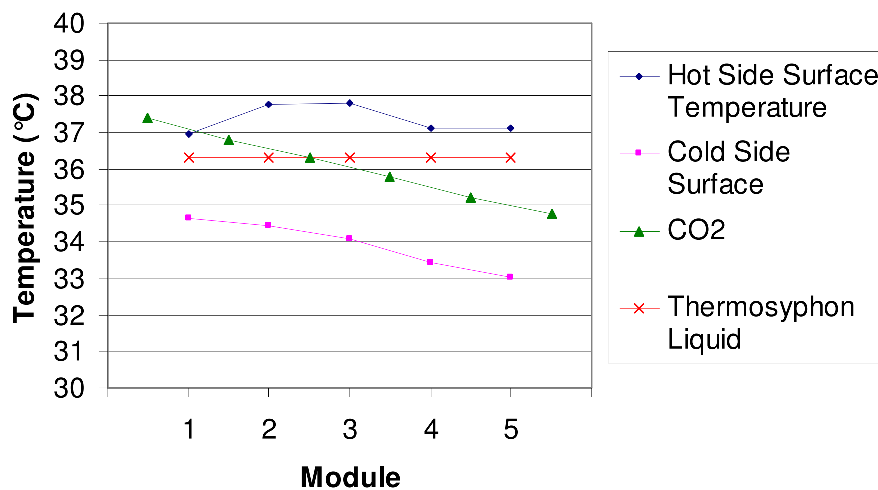

Figure 41: Temperature profile along the third generation subcooler.

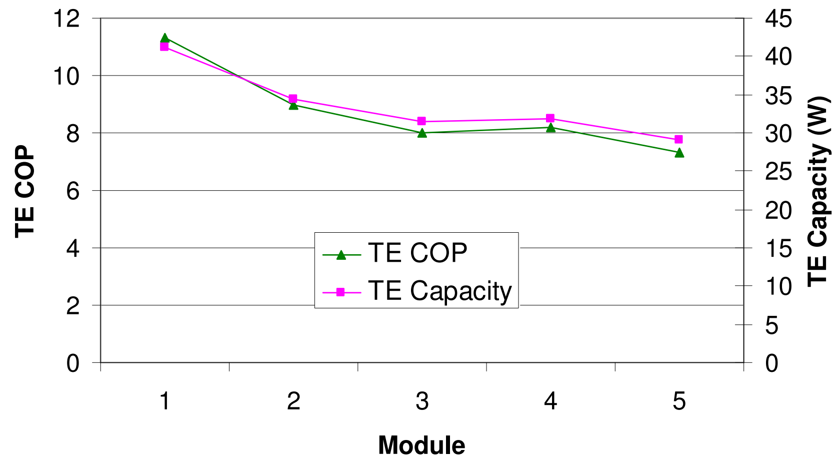

Figure 42: Module TE COP and Capacity for the third generation subcooler.

As performed on the second round test results, an estimate was made of the ΔT for the different thermal barriers within the third generation subcooler. Upon initial analysis, the CO_2 microchannel appeared to operate with a significantly lower total thermal resistance than estimated. It would appear that the Gnielinski correlation under predicted the heat transfer coefficient or that the assumed microchannel port diameter of 1.5 mm was too large. According to Liao and Zhao (2002) [28] constant property correlations such as those developed by Dittus-Boelter or Gnielinski do not accurately predict supercritical fluids, especially near the psuedocritical point. The large variations in the thermophysical properties with temperature require unique correlations and the inclusion of other forces. In particular, buoyancy effects, even in forced convection flows with Reynolds numbers $\sim 10^5$ cannot be neglected due to the large change in density and viscosity with temperature. Liao and Zhao (2002) [28] proposed a correlation for cooling of supercritical fluids near the psuedocritical point as shown in Equations 15 and 16. The nondimensional parameters Nu, Re, Pr, and Gr represent the Nusselt number, Prandtl number, Reynolds number, and Grashof number, respectively. In this equation, ρ is the

fluid density. The subscript w and b indicate whether the properties are evaluated at the wall temperature or the bulk mean temperature.

$$Nu_w = 0.128 \mathrm{Re}_w^{0.8} \mathrm{Pr}_w^{0.3} \left(\frac{Gr}{\mathrm{Re}_b^2} \right)^{0.205} \left(\frac{\rho_b}{\rho_w} \right)^{0.437} \left(\frac{\overline{C_p}}{C_{pw}} \right)^{0.411} \quad \mathbf{(15)}$$

$$\overline{C_p} = \frac{h_b - h_w}{T_b - T_w} \quad \mathbf{(16)}$$

For the application of the TE Subcooler the CO_2 is being cooled from above by the TE modules. As the CO_2 comes in contact with the upper wall and cools, the density rises sharply, causing the fluid to sink and displace the warmer less dense fluid, driving it to the top. This tumbling motion that can be imagined causes an increase in the heat transfer coefficient that is not captured by more conventional correlations. The preceding correlation suggests that there is actually less of an advantage to reducing port diameter, as it will cause a reduction of the buoyancy effect and reduce the Nusselt number.

Table 7 gives the assumptions used in the analysis. The Tin-Silver solder was assumed to only affect the 2nd and 3rd module, with the thicknesses given. The thermosyphon temperature difference between the wall of the enhanced boiling surface and the liquid thermosyphon refrigerant was calculated by subtracting the contribution of the TIM, copper, and solder from the total temperature difference between the hot side surface temperature and the refrigerant.

Figure 43 gives the contributing temperature differences. Since the approach temperature of the gas cooler was larger than the previous tests, the temperature difference between the fluids was negative until the third module. Due to the use of the microfin enhanced

boiling surface the contribution of the pool boiling was significantly reduced. The TIM still constituted a significant temperature difference although somewhat reduced. The largest contribution came from the convection to the CO_2 within the microchannels.

Table 7: Parameter assumptions for ΔT calculation.

Parameter	CO_2 Side	Thermosyphon Side
TIM Thickness (mm)	0.20	0.20
TIM Conductivity (W/mK)	8	8
Aluminum Thickness (mm)	1.25	-
Aluminum Conductivity (W/mK)	236	-
Copper Thickness (mm)	-	3.2
Copper Conductivity (W/mK)	-	400
Tin – Silver Solder Thickness (mm)	-	0.3,0.6
Brazing Alloy (W/mK)	-	32
HTC Correlation	Liao and Zhao (2002)	

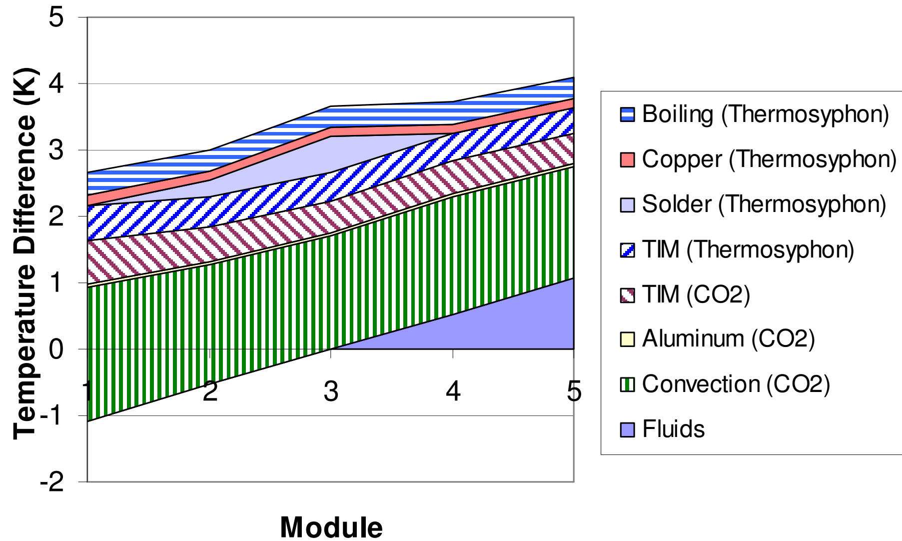

Figure 43: Temperature difference contributions for the third generation subcooler.

3.2: Modeling Results

3.2.1: TE Subcooler Performance Enhancement

The performance for the third generation subcooler predicted by the TE Subcooler model was compared against the experimentally measured TE capacity and TE COP for the third generation subcooler. The inputs included the inlet temperature and pressure of the CO_2, mass flow rate, and supply current. The temperature of the thermosyphon refrigerant was determined from the hot side heat rejection rate using a power law curve fit of the experimental data. The thermal resistance of the enhanced boiling surface was determined from the total heat flux in a similar manner. The other thermal resistances were calculated using the same assumptions given in Table 7, except for the thermal interface material. Since it is difficult to predict the exact thermal resistance of the TIM, the thickness was increased by 0.05 mm in order to better fit the experimental results. Figure 44 shows the calculated TE capacity and COP versus the measured values. All twelve cases were within 9% of the measured values. Nine of the 12 capacities calculated and 8 of the 12 TE COP's calculated were within 5% of the measured values.

As discussed previously there are multiple contributing thermal barriers to the total temperature difference across the module. In Section 3.1.3.2 the ΔT from each thermal barrier was quantified for the third generation subcooler. In order to achieve a greater TE COP it is necessary to reduce or in some cases eliminate these thermal barriers.

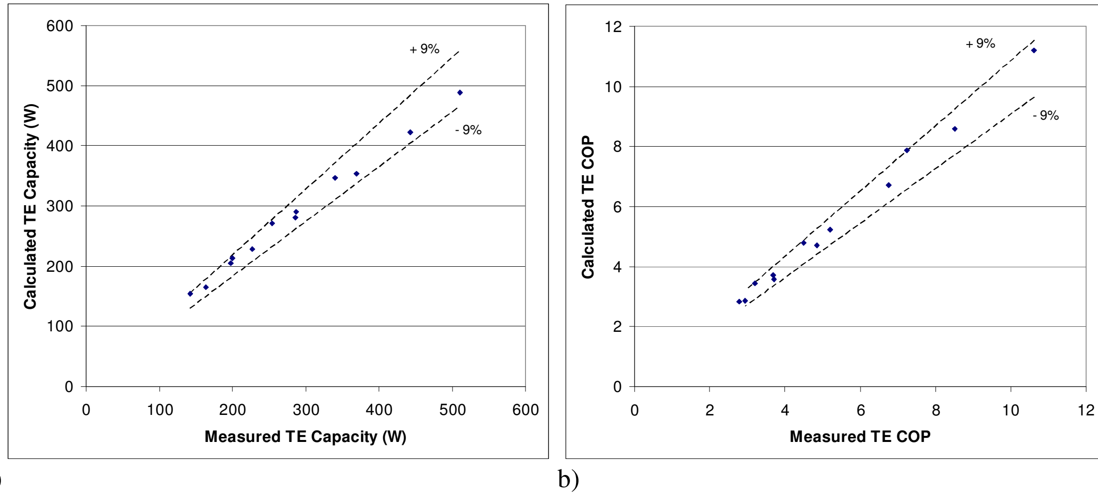

a) b)

Figure 44: Calculated versus measured TE capacity (a) and TE COP (b) for the third generation subcooler.

Although not the largest contributing ΔT, the TIM still represents a significant portion of the total ΔT_m. There are two options which can eliminate the use of thermal grease such as Arctic Silver. Both options require additional processing during module fabrication. The first method involves metallizing the ceramic surface of the TE module. This can be accomplished by sputtering nickel and copper and then a thin layer of gold to inhibit oxidation, with a total thickness of approximately 0.03 mm. This process is currently performed by Marlow, Inc. for some of their TE modules. It would allow for the use of a liquid metal TIM such as Liquid Pro or a low temperature solder. The rated maximum process temperature of the TE modules is 150°C, which would make a limited number of solders available. There are indium based solders with melting temperatures as low as 118°C. Because of thermo-mechanical stresses involved with soldering it would be necessary to solder both the hot and cold surfaces to their respective heat exchangers in one step or solder one surface and use Liquid Pro or another similar TIM for the other. This would effectively reduce the thermal resistance of the interface for each module from 0.011 K/W to 0.002 K/W.

It may also be possible to integrate the TE elements directly onto one of the heat exchangers. If the microchannel, for instance, were constructed out of a ceramic material that is both electrically insulating and thermally conductive, the thermoelectric elements could be mounted directly to the exterior surface. Beryllium Oxide, which is a common ceramic used in thermoelectric modules, has a thermal conductivity of approximately 270 W/mK at room temperature, which is greater than Aluminum. The tensile strength is also sufficient for a high pressure application. The total thermal resistance of the microchannel including the interface for each module could be reduced from 0.017 K/W to 0.004 K/W assuming a microchannel outer wall thickness of 1 mm.

The largest contributors to the total ΔT was the convection to the working fluid. During assembly it was necessary to have a small gap between the modules along the heat exchangers. If that gap was increased slightly, a heat spreading effect would result, which would increase the heat transfer surface area. Insulation within the gap would minimize any heat transfer from the hot surface of the heat rejection heat exchanger to the cold surface of the microchannel.

The thermal resistance of the pool boiling was successfully reduced using a microfinned enhanced boiling surface. In order to reduce the total thermal resistance of the thermosyphon loop, it would be necessary to employ a thermosyphon condenser with an internal enhanced condensing surface as developed by Webb et al (1998) [7]. Reducing

the condenser thermal resistance will increase the effectiveness of the heat sink and decrease the hot side surface temperature of the module.

The performance of a TE Subcooler with the modified design described above was estimated using the TE Subcooler model. The inlet conditions were assumed to be the same as the third generation subcooler test case with 4 A supply current at a discharge pressure of 9,200 kPa. The TE COP was improved from 8.73 to 10.22 with a corresponding increase in TE capacity from 168 W to 190 W. With 10 modules at a supply current of 3 A the calculated TE COP was 10.44 with a capacity of 231 W. The first and third subcooler combined had a measured TE COP of 8.67 with a capacity of 195 W at the same supply current and inlet conditions.

In order to assess the impact of an improved TE Subcooler design on the system performance a simplified CO_2 system model was developed. The compressor power, mass flow rate, gas cooler outlet temperature and pressure drop were estimated from the experimental data using best fit second degree polynomials. The expansion valve was assumed to be isenthalpic. The suction pressure and superheat were held constant at 4,198 kPa and 11.1 K, respectively. The TE Subcooler model predicted the outlet conditions entering the expansion valve from the inlet conditions and supply current. The power demand of the thermoelectrics was added to the compressor power to calculate the total system COP.

Table 8: Theoretical system performance with improved TE Subcooler design.

	Baseline System (Maximum COP)	TE System (Maximum COP)	TE System (Maximum COP)
System COP	2.37	2.69 (+14%)	2.70 (+14%)
System Capacity (kW)	1.47	1.77 (+21%)	1.74 (+19%)
Discharge Pressure (kPa)	9,400	9,000	9,000
Compressor Power (kW)	0.620	0.559	0.559
Mass Flow Rate (g/s)	10.6	10.9	10.9
TE Supply Current (Amps)	-	5	4
Number of Modules	-	10	12
TE Capacity (kW)	-	0.388	0.360
TE COP	-	6.37	7.59
GC/TE Outlet Temperature (°C)	37.4	31.9	32.5

As discussed previously, along with discharge pressure and supply current, the number of modules in the subcooler must also be optimized. Table 8 shows the system performance for the baseline system, a TE Subcooler system with 10 modules, and a TE Subcooler system with 12 modules. There is essentially no additional improvement by increasing the number of modules from 10 to 12. Further increases result in a decrease in system COP. The theoretical TE Subcooler System improves the system COP by 14% compared to the 10% improvement shown experimentally.

3.2.2: Expander-TE Subcooler System

As discussed in section 1.2.2 there are many methods employed which have the potential to improve the efficiency of a CO_2 system. One such method is the use of an expander in place of an expansion device. As it turns out there is an attractive combined effect from using TE Subcooler and expander in concert. The schematic of an Expander-TE Subcooler system is shown in Figure 45. The expander is coupled to a generator which would provide the necessary power for the TE Subcooler. In this way the expander would not need to be directly coupled to the compressor, avoiding heat transfer concerns and

allowing for independent control of the expander speed. The TE Subcooler would require no additional power besides that which is provided by the expander. Therefore, capacity gains would require no additional power and would result in greater improvements in COP.

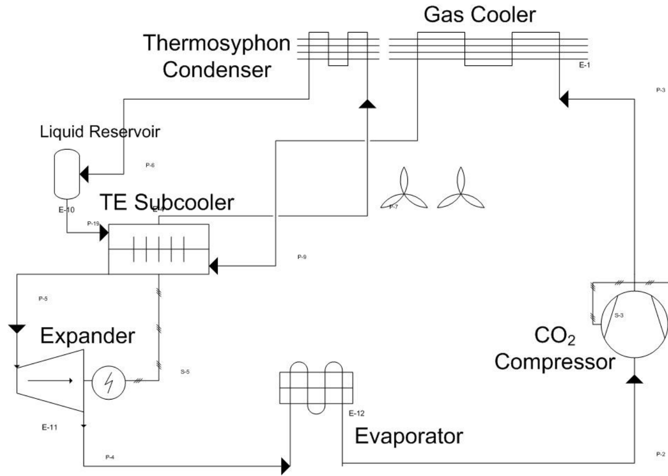

Figure 45: Schematic diagram of a refrigeration system with an Expander-TE Subcooler.

In order to quantify the potential of such a system a simplified expander model was integrated into the system model described above. The expander was modeled with a constant volumetric, indicated, mechanical and generator efficiency. The electrical power produced by the expander was calculated using Equation 17. The expander efficiencies are given in Table 9. The TE Subcooler was assumed to be the same as that which is discussed in the previous section.

$$P_{Exp} = \eta_{gen}\eta_{mech}\eta_{ind}\eta_{vol}(h_{inlet} - h_{outlet,s}) \quad \textbf{(17)}$$

Table 9: System assumptions

Expander indicated efficiency	70%
Expander volumetric efficiency	98%
Expander mechanical efficiency	95%
Generator efficiency	95%

The Expander-TE system is compared with the baseline system and an expander only system in Table 10. The expander only system assumes a direct couple between the expander and the compressor. Any power produced by the expander will decrease the power required by the compressor. For the expander only system the generator efficiency was assumed to be 1. As with any CO_2 system the discharge pressure was optimized to find the maximum COP for all cases. Number of modules for the Expander-TE System was also optimized. The supply current is determined by the expander power and the voltage drop of the thermoelectric modules.

The primary benefit of the TE Subcooler is to increase the capacity of the baseline system. The primary benefit of the expander is to decrease the power consumption of the compressor and therefore increase the COP of the baseline system. When combined, the Expander-TE Subcooler provides both increases in capacity and COP. The TE Subcooler provides the additional capacity and because no additional power is required, an increase in COP results.

Table 10: COP and capacity of three different systems

	Baseline System	Expander-TE System	Expander System
System COP	2.37	3.07 (+30%)	2.86 (+21%)
System Capacity (kW)	1.47	1.82 (+24 %)	1.56 (+6%)
Discharge Pressure (kPa)	9,400	8,900	9,400
Compressor Power (kW)	0.620	0.593	0.620
Expander Power (kW)		0.057	0.076
Mass Flow Rate (g/s)	10.6	10.99	10.6
TE Supply Current (Amps)	-	4.42	-
Number of Modules	-	12	-
TE Capacity (kW)	-	0.410	-
TE COP	-	7.14	-
GC/TE Outlet Temperature (°C)	37.4	32.3	37.4

Figure 46 shows the P-h diagrams for the four systems modeled. The available power that can be produced by the expander is reduced with the use of the TE Subcooler. The decrease in discharge pressure reduces the pressure ratio through the expander. Regardless, the Expander-TE system operates more efficiently and provides a greater cooling capacity than any of the other systems.

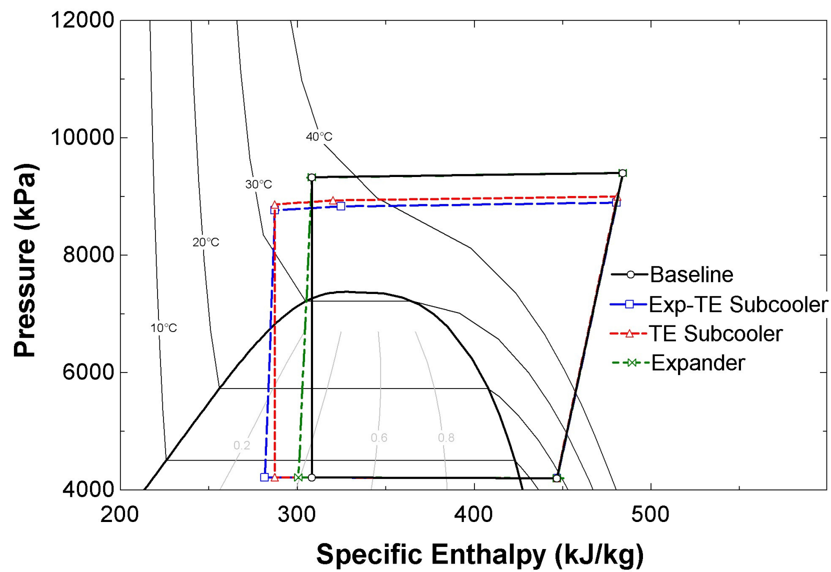

Figure 46: Pressure-enthalpy chart for four different systems with and without a TE Subcooler and an expander.

Chapter 4: Conclusions and Future Work

4.1: Conclusions

A TE Subcooler is a device which utilizes TE modules to cool refrigerant exiting a condenser or gas cooler to temperatures below ambient. By reducing the enthalpy of the refrigerant entering the evaporator, the system capacity is increased. When operated at a TE COP greater than the baseline system the system COP is also increased. For a CO_2 transcritical cycle a TE Subcooler will allow the high side pressure to be reduced, resulting in a greater COP improvement. The performance of TE Subcooler is dependent upon the thermal resistances between the cold side of the TE modules and the refrigerant, the thermal resistances between the hot side of the TE modules and the heat rejection fluid and the temperature difference between the two fluids. Three TE Subcoolers were tested utilizing a thermosyphon loop to reject heat.

A first generation TE Subcooler from a previous study was tested in a transcritical CO_2 cycle in order to experimentally verify the performance improvement. At a suction pressure of 4,198 kPa, the system COP was increased by 5% with a corresponding 9% increase in capacity. The 10 module TE Subcooler with a supply current of 4 Amps provided 204 W of cooling at a TE COP of 4.84. Under an increased supply current of 6 Amps, the TE Subcooler was able to increase the capacity of the system by 15% at comparable system COP to that of the baseline.

A second generation TE Subcooler was designed and fabricated. Unfortunately, due to complications during the fabrication process, the performance of the second generation

subcooler was unable to exceed that of the first generation subcooler. At a suction pressure of 2,906 kPa the first generation subcooler with 5 modules at a supply current of 6 Amps was able to increase the system COP by 8% with a corresponding 12% increase in capacity. By utilizing both the first and second generation subcooler in series at the same supply current the system capacity was increased by 15% at a comparable COP as the baseline system.

Finally, a third generation subcooler was fabricated and tested with the first generation subcooler in series. At a suction pressure of 4,198 kPa an increase in system COP of 10% was achieved with a corresponding 13% increase in capacity. The 10 module combined TE Subcooler at a supply current of 3 Amps provided 179 W of subcooling at a TE COP of 8.66. By increasing the supply current to 7.5 Amps a capacity improvement of 24% was achieved at comparable COP as the baseline system.

Testing was performed over a range of discharge pressures in order to find the maximum COP with and without the TE Subcooler. An optimum discharge pressure exists for the baseline system at a given suction pressure and ambient temperature. The TE Subcooler TE COP decreases with increasing discharge pressure due to the following:

1. Increased discharge pressure reduces the temperature at the outlet of the gas cooler leading to a larger temperature difference between the CO_2 and heat rejection fluid.
2. The specific heat of CO_2 decreases with increasing discharge pressure leading to greater reduction of the CO_2 temperature over the length of the subcooler, which

further increases the temperature difference between the fluids. The reduced specific heat also reduces the Prandtl number and the convective heat transfer coefficient.

3. The mass flow rate of the CO_2 decreases with greater pressure ratios, causing a reduction in the heat transfer coefficient within the subcooler as well as increasing the temperature difference as discussed in number 2.

The optimum discharge pressure for the system with the TE Subcooler is therefore a balance between the effects of discharge pressure on the baseline system and the effects of pressure on the TE Subcooler. The total system COP can be divided into two components as shown in Equation 18. The two ratios of capacity to total power are plotted versus discharge pressure in Figure 47. The optimum discharge pressure is found when the sum of the two terms is at a maximum.

$$COP_{sys} = \frac{Q_{Baseline} + Q_{TE}}{P_{cmp} + P_{TE}} = \frac{Q_{Baseline}}{P_{cmp} + P_{TE}} + \frac{Q_{TE}}{P_{cmp} + P_{TE}} \quad \textbf{(18)}$$

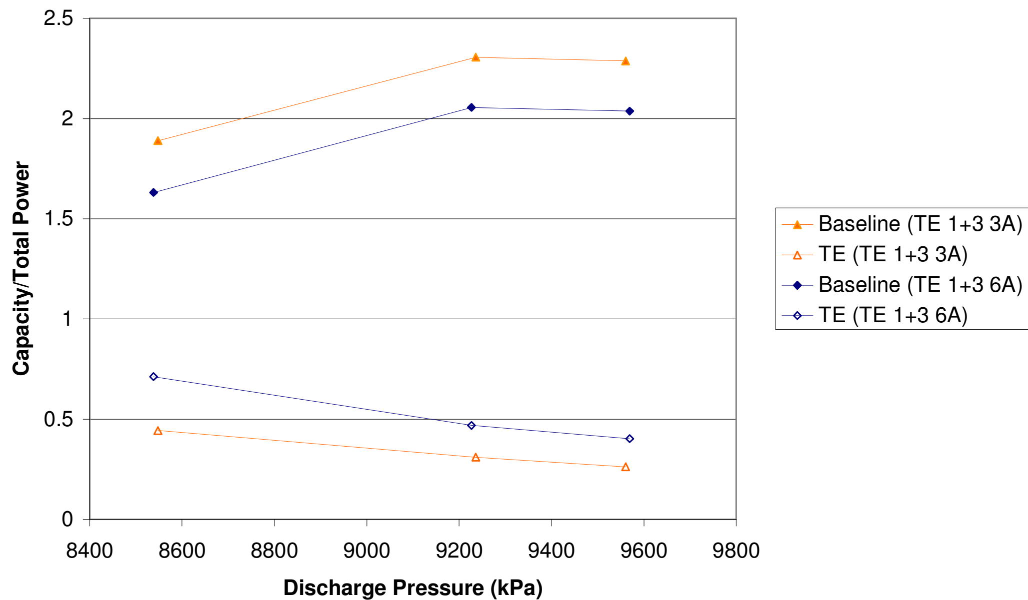

Figure 47: Contributions to the total system COP from the baseline and TE Subcooler.

The TE COP of the TE Subcooler is equal to the total cooling capacity of the modules over there total power consumption. As the capacity of the TE Subcooler is increased, either by increasing the supply current or the number of modules, the TE COP is reduced due to the following:

1. Increased supply current results in greater joule heating and power consumption of the thermoelectric modules.
2. Increased capacity results in a greater reduction in the CO_2 temperature causing an increased temperature difference between the fluids.
3. Increased heat flux causes greater temperature difference between the heat exchanger surfaces and the fluid on both sides of the subcooler.
4. Increased heat rejection rate causes an increase in the temperature and pressure of the thermosyphon refrigerant. The thermal resistance of the thermosyphon does increase with increased heat rate, but not enough to keep the temperature and pressure constant.
5. As the CO_2 is cooled the viscosity of the fluid increases causing an increase in the viscous stress and viscous sublayer thickness increasing thermal resistance of the convection with the microchannel wall.
6. As the CO_2 is cooled the specific heat decreases resulting in reduced thermal diffusion through the fluid channel and further increasing the thermal resistance of the convection with the microchannel wall.

There are a number of challenges inherent in the systems studied in this project. Carbon dioxide transcritical systems operate at extremely high pressure which requires careful

attention to safety, particularly when designing and fabricating new components. The thermodynamic properties of CO_2 near the critical point have large variations with temperature, making measurement uncertainty an important aspect of experimental design. Additionally, small changes in air flow rates and temperatures can have large effects on system performance and can negate or mask the true performance of the system being tested. Due to the large oil circulation rates of CO_2 systems, energy balance calculations can often be difficult. Thermosyphon systems have there own set of challenges. Refrigerant charge can have a significant impact on thermosyphon performance and requires a reliable and repeatable charge optimization process. As seen from the results the fabricated TE Subcooler often did not match the intended design. Difficulties in the fabrication process were common, but decreased as a greater understanding was reached. The TE modules themselves operated as expected without fault or failure.

A TE Subcooler model was developed and used to estimate the contributions of the various thermal resistances to the ΔT_m. The greatest contribution was identified as the convection to the CO_2 as well as the temperature difference between the CO_2 and heat rejection fluid at the end of the Subcooler. The combined effect of the TIM on both sides of the module also plays a significant role.

Design improvements over the third generation subcooler were identified. The integration of the TE modules into the CO_2 heat exchanger is possible if the heat exchanger is constructed from a high thermally conductive and electrically insolating material. This

would effectively remove the need for a TIM on at least one side of the TE modules. Sputtering a metal film on the heat rejection side of the modules would allow the use of a high thermal conductivity TIM such as a low temperature solder or liquid metal. Finally, along with the enhanced boiling surface an enhanced condensing surface would reduce the thermal resistance of the thermosyphon condenser.

A system model was developed using experimental results to quantify the performance improvement of a TE Subcooler utilized the design improvements discussed above. The greatest improvement in system COP was estimated to be 14% with a corresponding increase in capacity of 21%.

Through the experimental and theoretical analysis it was observed that although significant improvements in COP can be achieved, the capacity improvement potential is greater. Alternative power sources represent great potential in combination with a TE Subcooler. The use of an expander was identified as a method to power the TE Subcooler, thus providing increased capacity without an increase in power consumption and therefore leading to greater COP improvements. The performance of an Expander-TE Subcooler system was estimated using the system model, showing a 30% improvement in COP with a corresponding improvement in capacity of 24%.

Yet another alternative power source is solar energy. Photovoltaic solar panels produce DC electric power that could be used to power the TE Subcooler. Building cooling load generally increases with solar radiation as would the power produced by a solar panel. If

connected to a TE Subcooler the capacity of the air conditioning system could increase with the increased load. If the system were correctly sized the increase in capacity could match the increase in cooling load.

4.2: Recommendations for Future Work

In order to validate the theoretical performance improvement shown for an Expander-TE Subcooler system, an experimental investigation is necessary. Difficulty arises in the procurement of an expander, which is still in the development phase.

The fabrication of a microchannel heat exchanger with integrated thermoelectric modules requires additional development. The heat rejection thermosyphon evaporator in future research should be constructed with a visualization section to determine the boiling characteristics. Additionally, the development and application of a thermosyphon condenser with an enhanced condensing surface was not addressed in the current study, but has a significant impact on the TE Subcooler performance. Finally, the integration of the thermosyphon condenser into the gas cooler assembly in a parallel arrangement should be considered as the research moves beyond the concept validation phase.

There is also additional theoretical work that would assist in the development of a TE Subcooler. As discussed previous the TE modules themselves can be optimized for a particular application. Future modeling efforts should focus on the optimization of the TE module size and heat flux, as well as the semiconductor shape factor, λ, for a subcooling

application. Consideration must be given to the additional cost and difficulty in the fabrication of newly developed modules.

Finally, a theoretical investigation of the potential of a TE Subcooler powered by photovoltaics may lead to further increases in COP with the additional advantages inherent in solar cooling.

4.3: Summary of Completed Tasks and Key Findings

1. Two TE Subcoolers were designed and fabricated.
2. A small CO_2 transcritical vapor compression cycle refrigeration system was designed and built to test the TE Subcoolers. The maximum COP and capacity of the baseline system and TE Subcooler systems was measured at two suction pressures by optimizing both discharge pressure and TE supply current.
3. A COP improvement of 8% with a corresponding increase in capacity of 12% was achieved utilizing the first generation subcooler for the low suction pressure case. A COP improvement of 10% with a corresponding increase in capacity of 13% was achieved utilizing the first and third generation subcoolers in series for the high suction pressure case.
4. A number of factors were identified which cause a reduction in the performance of the TE Subcooler as the discharge pressure and supply current is increased.
5. A TE Subcooler model was developed to estimate the impact of the contributing thermal resistances on the TE Subcooler performance. The convective heat transfer to

the CO_2 and the temperature difference between the CO_2 and the heat rejection fluid were identified as the greatest thermal barriers.

6. Improvements to the TE Subcooler design were proposed and the potential impact of such improvements was estimated. The estimated system COP improvement was 14% with a corresponding increase in capacity of 21%.
7. The use of an expander in place of an expansion valve to power the TE Subcooler was proposed and the improvement potential was estimated using a system model. The estimated system COP improvement was 30% with a corresponding increase in capacity of 24%.

Bibliography

[1] Gurevich, Y. and Logvinov, G., 2005, Physics of thermoelectric cooling, Semiconductor Science and Technology, 20, November 2005, pp. R57 – R64.

[2] Nabi, A. and Asias, A., 2005, A Simple Experimental Technique for the Characterization of the Performance of Thermoelectric-Coolers beyond 100°C, 21st IEEE SEMI-THERM Symposium. 2005.

[3] Bass, J., Allen, D., Ghamaty, S., & Elsner, N. "New Technology for Thermoelectric Cooling." 20th IEEE SEMI-THERM Symposium. 2004.

[4] Goldsmid, H. J. "Bismuth – Thermoelectric Material of the Future?" International Conference on Thermoelectrics. (2006) 5-10.

[5] Xuan, X.C., Ng, K.C., Yap, C., Chua, H.T. "The maximum temperature difference and polar characteristic of two-stage thermoelectric coolers." Cryogenics. 42 (2002) 273-278

[6] Chein, R., Chen, Y. "Performance of thermoelectric cooler integrated with microchannel heat sinks." International Journal of Refrigeration. 28 (2005) 828-839

[7] Webb, R.L., Gilley, M.D., Zarnescu, V. "Advanced Heat Exchanger Technology for Thermoelectric Cooling Device." Journal of Electric Packaging. 120 (1998) 98 – 105

[8] Riffat, S. & Qiu, G. "Design and characterization of a cylindrical, water-cooled heat sink for thermoelectric air-conditioners." International Journal of Energy Research. 30 (2006) 67-80

[9] Kohsokabe, H., Funakoshi, S., Tojo, K., Nakayama, S., Kohno, K., and Kurashige, K. "Basic Operating Characteristics of CO_2 Refrigeration Cycles with Expander-Compressor Unit." International Refrigeration and Air Conditioning Conference at Purdue July 17-20, 2006.

[10] Boewe, D. Yin, J., Park, Y.C., Bullard, C.W., Hrnjak, P.S. "The role of suction line heat exchanger in transcritical R744 mobile A/C systems." SAE International Congress and Exposition. (1999)

[11] Winkler, J., Aute, V., Yang, B., Radermacher, R., 2006, Potential Benefits of Thermoelectric Elements used with Air-Cooler Heat Exchangers, Proc. International Refrigeration and Air Conditioning Conference, West Lafayette, IN., R091.

[12] Muehlbauer, J. Presentation to the Alternative Cooling Technologies & Applications Consortium, Center for Environmental Energy Engineering. September 2006.

[13] Suss, J., Veje, V. "Development and Performance Measurements of a Small Compressor For Transcritical CO_2 Applications." International Compressor Engineering Conference at Purdue. July 12-15, 2004.

[14] Gnielinski, V., Int. Chem. Eng., Vol. 16, p. 359, 1976

[15] Schlichting, H. *Boundary Layer Theory*, 6th ed. McGraw-Hill, New York, 1968. in Incropera, F.P. and DeWitt, D.P., *Introduction to Heat Transfer*, 4th Ed., Wiley, 2002.

[16] W.M. Rohsenow, "A Method of Correlating Heat Transfer Data for Surface Boiling of Liquids," Trans. ASME (74): 969, 1952.
[17] Lee, J., 2003, Experimental and Theoretical Investigation of Oil Retention in a Carbon Dioxide Air-Conditioning System, Ph. D. Dissertation, University of Maryland.
[18] R. Span and W. Wagner, A New Equation of State for Carbon Dioxide Covering the Fluid Region from the Triple-Point Temperature to 1100 K at Pressures up to 800 MPa, J. Phys. Chem, Ref. Data, Vol. 25, No. 6, 1996.
[19] Incropera, F.P. and DeWitt, D.P., *Introduction to Heat Transfer*, 4th Ed., Wiley, 2002.
[20] ANSI/ARI Standard 540 (1999)
[21] Kays, W., Crawford, M., & Weigand, B. *Convective Heat and Mass Transfer,* 4th Edition, McGraw-Hill (2004).
[22] Hwang, Y., Class Notes, ENME635 Cooling, Heating and Power Integration. University of Maryland, College Park, MD. Spring 2007.
[23] Yaun, L., Joshi, Y., & Nakayama, W. "Effect of Condenser Location and Imposed Circulation on the Performance of a compact Two-Phase Thermosyphon." Microscale Thermophysical Engineering. 7 (2003) 163-179.
[24] Khodabandeh, R., Palm, B. "An Experimental and Numerical Investigation of Pressure Drop in a Two Phase Thermosyphon System." Inter Society Conference on Thermal Phenomena. (2000) 333-339
[25] Webb, Ralph L., 1994, *Principles of Enhanced Heat Transfer.* John Wiley & Sons, Inc., New York, NY. p. 311 – 371.
[26] Thome, J. *Enhanced Boiling Heat Transfer*. Hemisphere Publishing Corp., New York.
[27] Wolverine Tube, Inc. Engineering Data Book, http://www.wlv.com/products/databook/ch5_4.pdf
[28] Liao, S.M., & Zhao, T.S. "Measurement of Heat Transfer Coefficients From Supercritical Carbon Dioxide Flowing in Horizontal Mini/Micro Channels." Journal of Heat Transfer. 124 (2002) 413-420
[29] Span, R., & Wagner, W. "A New Equation of State for Carbon Dioxide Covering the Fluid Region from the Triple-Point Temperature to 1100 K at Pressures up to 800 MPa," J. Phys. Chem, Ref. Data, Vol. 25, No. 6, 1996.
[30] CoilDesigner Version 3.1.20072.418. Copyright © 2004-2008 Center for Environmental Energy Engineering, University of Maryland
[31] LabVIEW 8.2, Copyright © 2006 National Instruments.
[32] McLinden, M., Klein, S. A., Lemmon, E. W., and Peskin, A. P., 1998, "NIST Thermodynamic and Transport Properties of Refrigerants and Refrigerant Mixtures-REFPROP," Version 6.01, National Institute of Standards and Technology, USA.
[33] Mostinski, I.L. 1963. "Application of the rule of corresponding states for the calculation of heat transfer and critical heat flux." Teploenergetika 4:66; English abstract, Br. Chem. Eng. 8(8):580 (1963).
[34] Radermacher, R. and Yang, B. Innovative thermoelectrics-assisted vapor-compression refrigeration systems, PS-2005-076, 2005.